EUROPEAN JOURNAL OF COMPUTATIONAL MECHANICS, 2017
VOL. 26, NOS. 5–6, 473–507
https://doi.org/10.1080/17797179.2017.1354576

Taylor & Francis
Taylor & Francis Group

Dynamic behaviours of spinning pre-twisted Rayleigh micro-beams

K. B. Mustapha

Department of Mechanical, Materials and Manufacturing Engineering, University of Nottingham Malaysia Campus, Semenyih, Malaysia

ABSTRACT

Developments in micro-systems' operations rely on identifying and controlling the dynamic responses of micrometre-scale elements. Pre-twisted micro-elements feature prominently in these systems, yet very little is known about the interacting effect of motley factors on their behaviours. Presented here is a model of pre-twisted micro-beams that accounts for the coupling of scale-dependent, rotary inertia and spinning effects in vibratory and wave propagation analyses. In tackling the problem, the system's physical domain is transformed into the mathematical realm via a scale-dependent micro-continuum theory, while its time evolution is captured by Hamiltonian mechanics. Analytic expressions are obtained for the long-wavelength limit and dispersion relations. The spectrum relations of the waves are established from an octic characteristics equation (which, being in violation of the Abel–Ruffini theorem is treated numerically). Splitting of the waves within the system is observed, and the frequencies of the split shift for altered values of the pre-twist angle and rotary inertia effect. Thinner, highly pre-twisted micro-scale beams experience a widening (narrowing) of the difference between the two phase speeds (group velocities) of the waves. Further, pre-twisting lowers the natural frequencies associated with odd-numbered modes of vibration of the element, while the small-scale effect strongly affects the higher vibration modes.

ARTICLE HISTORY
Received 24 February 2017
Accepted 10 July 2017

KEYWORDS
Pre-twisted micro-scale beam theory; elastic wave propagation; spectrum curve; spinning dynamics; Rayleigh beam theory; Rayleigh–Ritz method; modified couple stress theory

1. Introduction

An expansive volume of technical literature exists on the topic of pre-twisted rods, beams, plates and shells. The seminal work of Love (1927), as reported by Rosen (1991), is credited with the initiation of the theory of elasticity for the modelling of twisted rods. Numerous research efforts have since been devoted to the analyses of structures with varying degrees of pre-twisting.

Excellent treatments of the subject matter include studies that can be classified broadly into three categories. In the first category are studies in which the

CONTACT K. B. Mustapha KhameelB.Mustapha@nottingham.edu.my, kham0002@ntu.edu.sg

static bending of pre-twisted rods and beams is reported: Zickel (1952)), Carnegie (1957), Houbolt and Brooks (1957), Goodier and Griffin (1969), Reissner and Wan (1971), Guglielmino and Saccomandi (1996). The second category relates to studies in which the structural vibration and stability of pre-twisted one-dimensional, two-dimensional and three-dimensional structures are investigated. A partial list of this includes studies by: Troesch, Anliker, and Ziegler (1954), Carnegie (1959, 1964), Dawson (1968)), Fu (1974), Rao (1976), Subrahmanyam, Kulkarni, and Rao (1981), Leissa, MacBain, and Kielb (1984), MacBain, Kielb, and Leissa (1985), Qatu and Leissa (1991)), Hu and Tsuiji (1999), Chen and Keer (1993), Liew, Lim, and Ong (1994), Lim and Liew (1995), Balhaddad and Onipede (1998), Yardimoglu and Inman (20040, Song, Jeong, and Librescu (2000), Lin, Wang, and Lee (2001), Sahu, Asha, and Mishra (2005), Banerjee (2001, 2004), Leung and Fan (2010) and Sinha and Turner (2011). The emphasis of most of the aforementioned studies is driven by applications in turbine-compressor, turbo-chargers, helicopter blading, wind power generators, air-moving equipment etc. In the third category are those studies that focus on use of the pre-twisted beam model in characterising the mechanical behaviour of high-speed machining tools. A few of the studies in this latter category deserves to be mentioned. Tekinalp and Ulsoy (1989) developed a mathematical model of oscillating drill bits utilising the pre-twisted Euler–Bernoulli beam theory. Liao and Dang (1992) analysed the transverse vibration and stability of a spinning orthotropic twisted beam for idealising the behaviour of conventional end mills. Young and Gau (2003) considered the effect of non-constant spin rates on the dynamic stability of pre-twisted beams under axial random forces. Huang and Kuang (2007) deployed the pre-twisted beam model to simulate the instability of drill bits in high-speed drilling processes, with consideration of the time-dependent nature of the thrust force and a moving Winkler-type elastic foundation. Filiz and Ozdoganlar (2011) presented a three-dimensional pre-twisted beam model with emphasis on the axial-bending-torsional dynamics of end mills. Hybrid analytical models for estimating the transverse vibration response of end mills were reported in Mustapha and Zhong (2013, 2012). Relying on the shear-deformable pre-twisted beam theory, Chen and Chen (2015) demonstrated the effect of axial pulsating loads and localised damage on the parametric instability of pre-twisted Timoshenko beams.

A new category of application is emerging in numerous areas in which micro-scale pre-twisted structures act as major components of the system. For instance, the pre-twisted micro-scale beam finds application in: micro turbomachinery and micromachining (Mindlin & Tiersten, 1962; Zhang & Meng, 2006); ultrasonic piezoelectronic motor (Liu, Friend, & Yeo, 2009; Wajchman, Liu, Friend, & Yeo, 2008); and biomedical devices (Watson, Friend, & Yeo, 2009). Most of the pre-twisted beam in these emerging applications have dimensions in the sub-millimetre range, yet existing studies have relied on models formulated using the classical continuum theory (CCT) to characterise their load-bearing capabilities and responses. Indeed, the pre-twisted beam models based on the CCT

have been reasonably accurate when employed to characterise the behaviour of pre-twisted structures with macro dimensions. However, the accuracy of such models becomes questionable for analysing the behaviour of ultra-thin micro-sized pre-twisted structure. In numerous studies, the mechanical behaviours of micro- and nano-scale elements have been confirmed to deviate from the predictions of the CCT (Mustapha, 2015; Mustapha & Wong, 2016). In short, the theory does not account for the established observations that as the thickness of nano- and micro-sized structures approaches their internal material length scales, their responses to external loads are susceptible to the occurrence of size-effect (Fleck & Hutchinson, 1993).

Currently, the quest to address the inclusion of size-effect in micro-structured materials has spawned increased research interests in enriched micro-continuum theories (Challamel, 2013; Mustapha & Hawwa, 2015; Shojaeian, Beni, & Ataei, 2016; Zeighampour & Beni, 2015), most of which rest on the works of the Cosserat brothers (Cosserat & Cosserat, 1909). Frequently, a good number of recent research studies employing these theories adopt any of the conception of: (a) the couple stress theory laid down by Mindlin and Tiersten (19620 and Toupin (1964)) in the 1960s; (b) the strain gradient theory reported and expanded, between the 1980s and 1990s, by Aifantis (1984, 1992) and Fleck and Hutchinson (1993), Fleck, Muller, Ashby, and Hutchinson (1994); or (c) the non-local Eringen's elasticity theory (Eringen & Edelen, 1972). From all these studies and allied works, a recurring theme that arises with the use of the enriched micro-continuum theories is the notorious problem of determining the ensuing material constants (called length-scale parameters) associated with micro-structured solids. In this regard, promising advancement in micro-bending, micro-torsion and nano-indentation tests has emerged as enablers (Deng, Peng, Lai, Fu, & Lin, 2017), and the significant progress made along this direction has allowed the extension of these theories to the modelling of complex micro-structured solids.

In the present study, the mechanical behaviour of spinning pre-twisted micro-scale beams with inertia effect and scale-dependent property is considered. The system's governing equation is derived through the combined frameworks of variational calculus and the modified couple stress theory (MCST) (Yang, Chong, Lam, & Tong, 2002). Many studies have relied on the minimalism of the MCST to formulate variationally consistent models for static, buckling and free vibration analyses of various microstructure-dependent structures (such as microtubules, micro-sized rods, micro-scale beams and plates) (Dehrouyeh-Semnani, Dehrouyeh, Torabi-Kafshgari, & Nikkhah-Bahrami, 2015; Dehrouyeh-Semnani, Mostafaei, & Nikkhah-Bahrami, 2016; Ghayesh, Farokhi, & Gholipour, 2017; Razavilar, Alashti, & Fathi, 2014; Şimşek & Reddy, 2013; Yang & Lakes, 1982). In principle, the MCST facilitates the characterisation of microstructural effect with just one material length-scale parameter (Ataei, Beni, & Shojaeian, 2016; Liang, Ke, Wang, Yang, & Kitipornchai, 2015; Yang et al., 2002; Zeighampour, Beni, & Mehralian, 2015). Accounting for the size-effect phenomenon is of primary

interest in providing an accurate interpretation of the process in which ultra-thin micro-sized pre-twisted structures are involved. To the best of the author's knowledge, the number of studies available in the literature that have considered the scale-dependent behaviour in the context of the dynamics behaviour of pre-twisted micro-scale beam is limited. The development of a model for the wave propagation behaviour of a pre-twisted micro-beam was presented in Mustapha and Zhong (2012). However, the capability of the model in (Mustapha & Zhong, 2012) is limited due to the non-consideration of the duo of rotary inertia and spinning effects. Recently, the vibro-buckling characteristics of rotating pre-twisted micro-beams with heterogeneous and homogeneous material properties were presented in Ghorbani Shenas, Ziaee, and Malekzadeh (2016), Ghorbani Shenas, Malekzadeh, and Ziaee (2017) and Mohammadimehr, Farahi, and Alimirzaei (2016). However, our understanding of the coupled effects of spinning, scale-dependent property and rotary inertia on both the wave propagation and the free vibration behaviours of these structures remains hazy.

The remainder of this paper illustrates the modest contribution of the present study to address this problem. In Section 2, we combine the principle of Hamiltonian mechanics and the variational formulation of the MCST to derive the mathematical model of spinning pre-twisted Rayleigh micro-scale beams, and some well-known simplified cases of the established model are also revealed for verification purposes. Section 3 details spectral analyses for wave propagation, and further features the analytic expressions for the cut-off frequencies of the full and simplified models. The free vibration study, employing the Rayleigh–Ritz method of solution for the model, is presented in Section 3. Section 5 summarises the observations from the analyses.

2. The perturbed field equations

2.1. Kinematic considerations, deformation measures and constitutive relations

The structural system under consideration comprises a spinning pre-twisted micro-scale beam whose three-dimensional model is shown in Figure 1. The schematic of a segment of the system and the adopted coordinate system used for the analyses are shown in Figure 2(a) and (b), respectively.

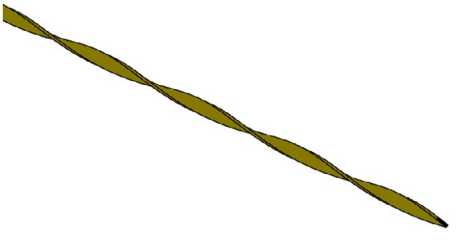

Figure 1. Three-dimensional model of a pre-twisted beam.

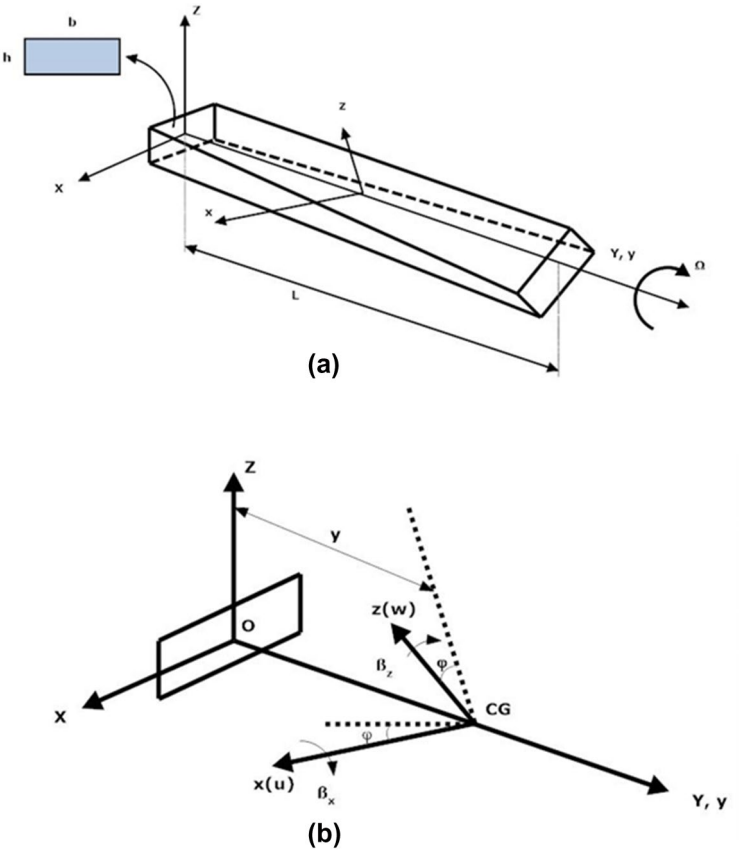

Figure 2. (a) a spinning pre-twisted micro-scale beam with the direction of spinning; (b) coordinate systems and rotation angles.

For modelling convenience, we assume that the cross-section of the pre-twisted micro-scale beam experiences no deformation in its own plane, and focuses on the small-strain analysis. Further, we establish reference frameworks by embossing the pre-twisted micro-scale beam with three coordinate systems: (i) the inertia coordinate system *XYZ*; (ii) the pre-twisted coordinate system *xyz*; and (iii) the reference frame $x'y'z'$ that spins with the micro-beam at a uniform spinning speed (Ω), which takes place about the beam's dominant structural axis. Moreover, the axes *Y*, *y* and y' coincide with the centreline of the pre-twisted beam. In the spirit of kinematical consideration, a generic point P_1 that lies in the cross section of the beam axis is assumed to move to P_2 when the structure is deformed by a system of externally applied loads. One may thus assume a generic displacement trial field ($\boldsymbol{u}$) under such a deformation in the form:

$$\boldsymbol{u} = \sum_{j=1}^{3} u_j e_j \tag{1}$$

where u_j (j = 1, 2, 3) are the components of the displacement at time t along the x, y and z-axes, respectively. For a coupled flexure–flexure deformation (with all motion assumed to be isothermal) in the two orthogonal planes, $\boldsymbol{u}$ is associated with the total displacement. To identify the components of the total displacement, it is assumed that the pre-twisted micro-scale beam (homogeneous and isotropic) has a twist angle φ, and a uniform rate of twist $\gamma = d\varphi/dy$. With this, the components of $\boldsymbol{u}$ in the x, y and z directions can be explicitly prescribed, following Banerjee (2001), as:

$$u_1 = u(y,t); \quad u_2 = -z(w' - \gamma u) - x(u' + \gamma w); \quad u_3 = w(y,t) \tag{2}$$

where u, v and w correspond to the displacements of a point of the pre-twisted micro-scale beam on the neutral line $Y = y = 0$. Moving from the pre-twisted frame of reference to the inertial frame of reference requires the use of the transformation relationship expressed as:

$$\vec{u}_{XYZ} = T_{\Omega} T_{\varphi} \vec{u}_{xyz} \tag{3}$$

where T_{Ω} and T_{φ} are transformation matrices defined as:

$$T_{\Omega} = \begin{bmatrix} \cos \Omega t & 0 & -\sin \Omega t \\ 0 & 1 & 0 \\ \sin \Omega t & 0 & \cos \Omega t \end{bmatrix}; \quad T_{\varphi} = \begin{bmatrix} \cos \varphi & 0 & -\sin \varphi \\ 0 & 1 & 0 \\ \sin \varphi & 0 & \cos \varphi \end{bmatrix} \tag{4a, b}$$

With Equation (4), the displacement components in the inertial frame (U, V and W, along X, Y and Z, respectively) can thus be written in terms of those in the pre-twisted coordinate system as:

$$U = u \cos \varphi + w \sin \varphi \tag{5}$$

$$W = -u \sin \varphi + w \cos \varphi \tag{6}$$

$$V = -(X \sin \varphi + Z \cos \varphi)(w' - \gamma u) - (X \cos \varphi - Z \sin \varphi)(u' + \gamma w) \tag{7}$$

where the spatial distance x and z in Equation (2) have been replaced accordingly in Equation (7).

Based on the MCST, the total strain energy $(\boldsymbol{\Pi}_s)$ generated by the deformation of the pre-twisted micro-scale beam is an assembly of the strain energy contribution of the Cauchy stress tensor $(\boldsymbol{\Pi}_{cs})$ and the strain energy contribution of the modified couple stress tensor $(\boldsymbol{\Pi}_{ms})$. This then leads to the total strain energy to be characterised by a quartet of tensors related as (Reddy, 2011; Yang et al., 2002):

$$\Pi_s = \Pi_{cs} + \Pi_{ms} = \frac{1}{2}\int_{\forall} (\boldsymbol{\sigma}:\boldsymbol{\varepsilon}) dV + \frac{1}{2}\int_{\forall} (\boldsymbol{m}:\boldsymbol{\chi}) dV \tag{8}$$

where the domain $\forall$ occupied by the pre-twisted micro-beam is taken to be an open set in $\mathbb{R}^3$. The terms $\boldsymbol{\varepsilon}$ and $\boldsymbol{\sigma}$ (in Equation 8) are the dilatation strain and the Cauchy stress tensors, respectively. Additionally, the tensors $\boldsymbol{m}$ and $\boldsymbol{\chi}$ refer to the deviatoric component of the couple stress and the symmetric curvature tensor, respectively. Equation (8) has to be supplemented by the following kinematic relations (i.e. Equations 9–11) and the non-classical constitutive equations expressed in Equations (12) and (13):

$$\boldsymbol{\varepsilon} = \frac{1}{2}\left[\nabla \boldsymbol{u} + (\nabla \boldsymbol{u})^{\mathrm{T}}\right] \tag{9}$$

$$\boldsymbol{\chi} = \frac{1}{2}\left[\nabla \boldsymbol{\theta} + (\nabla \boldsymbol{\theta})^{\mathrm{T}}\right] \tag{10}$$

$$\boldsymbol{\theta} = \frac{1}{2}\mathrm{curl}\, \boldsymbol{u} \tag{11}$$

$$\boldsymbol{\sigma} = \lambda \mathrm{tr}(\boldsymbol{\varepsilon})\mathbf{I} + 2G\boldsymbol{\varepsilon} \tag{12}$$

$$\boldsymbol{m} = 2\ell^2 \mu \boldsymbol{\chi} \tag{13}$$

where $\boldsymbol{u}$ and $\boldsymbol{\theta}$ denote the displacement and rotation vectors, respectively. It is noted that in Equation (12), the stress field is related to the displacement field with the aid of the material parameters λ (the bulk modulus) and G (the shear modulus), respectively. However, in Equation (13), the couple stress field is related to the displacement field through an additional material constant in the form of ℓ, which is the material length-scale parameter representing the microstructural effect. In subsequent derivations substitutions are made for λ in the form $\lambda = Ev/(1+v)(1-2v)$.

Given the nature of the displacement components in Equations (5)–(7), the only non-zero component of the strain tensor is ε_{yy} (based on the shear-rigid assumption), and this is obtained as:

$$\begin{aligned}\varepsilon_{yy} = {} & \gamma(Z\cos\varphi + X\sin\varphi)\left(\gamma w + u'\right) - \gamma(X\cos\varphi - Z\sin\varphi)\left(-\gamma u + w'\right) \\ & + (X\cos\varphi - Z\sin\varphi)(-\gamma w' - u'') + (Z\cos\varphi + X\sin\varphi)(\gamma u' - w'')\end{aligned} \tag{14}$$

Also from Equations (5)–(7) and (11), the two non-zero components of the rotation vector are:

$$\theta_x = -\gamma\cos\varphi\, u - \gamma\sin\varphi\, w - \sin\varphi\, u' + \cos\varphi\, w' \tag{15}$$

$$\theta_z = \gamma\sin\varphi\, u - \gamma\cos\varphi\, w - \cos\varphi\, u' - \sin\varphi\, w' \tag{16}$$

In a similar spirit, with Equations (10), (15) and (16), one obtains the following two (out of nine) components of the symmetric curvature tensor:

$$\chi_{xy} = \frac{1}{2}\sin\varphi(\gamma^2 u - 2\gamma w' - u'') + \frac{1}{2}\cos\varphi(-\gamma^2 w - 2\gamma u' + w'') \tag{17}$$

$$\chi_{yz} = \frac{1}{2}\cos\varphi(\gamma^2 u - 2\gamma w' - u'') + \frac{1}{2}\sin\varphi(\gamma^2 w + 2\gamma u' - w'') \tag{18}$$

Now, from the transformation matrix (and also Equations (5) and (6)), one can identify that:

$$z = Z\cos\varphi + X\sin\varphi \tag{19a}$$

$$x = X\cos\varphi - Z\sin\varphi \tag{19b}$$

Using Equation (19), we may then re-write Equation (14) as:

$$\varepsilon_{yy} = \gamma z\left(\gamma w + u'\right) - \gamma x\left(-\gamma u + w'\right) + x(-\gamma w' - u'') + z(\gamma u' - w'') \tag{20}$$

Assuming that the pre-twist angle is taken to be very small, then a truncated series expansion of cos φ and sin φ is:

$$\cos\varphi \approx 1 - \frac{\varphi^2}{2} + \frac{\varphi^4}{24} - \frac{\varphi^6}{720} + \ldots \tag{21a}$$

$$\sin\varphi \approx \varphi - \frac{\varphi^3}{6} + \frac{\varphi^5}{120} + \ldots \tag{21b}$$

Equation (21) is employed in Equations (17) and (18) to obtain a simplified expressions for χ_{xy} and χ_{yz} in the form:

$$\chi_{xy} = \frac{1}{2}\left(-\gamma^2 w - 2\gamma u' + w''\right) + \underline{\frac{1}{2}\varphi(\gamma^2 u - 2\gamma w' - u'')} \tag{22}$$

$$\chi_{yz} = \frac{1}{2}(\gamma^2 u - 2\gamma w' - u'') + \underline{\frac{1}{2}\varphi(\gamma^2 w + 2\gamma u' - w'')} \tag{23}$$

In what follows, the underlined terms in Equations (22) and (23) will be omitted in the energy equations in order to skirt the introduction of a torsional degree of freedom into the governing equation. With the help of the derived components of the tensors $\boldsymbol{\varepsilon}$ and $\boldsymbol{\chi}$, the strain energy functional becomes:

$$\Pi_s = \frac{1}{2}\int_0^L \int_A \left(E\left(x^2\left(\gamma^2 u - 2\gamma w' - u''\right)^2 + z^2\left(\gamma^2 w + 2\gamma u' - w''\right)^2\right)\right. \tag{24}$$
$$\left. + G\ell^2\left(-\gamma^2 w - 2\gamma u' + w''\right)^2 + G\ell^2\left(\gamma^2 u - 2\gamma w' - u''\right)^2\right) dA dx$$

The kinetic energy term, considering the effect of spinning and rotary inertia, is of the form:

$$\Pi_K = \frac{1}{2}\int_0^L \int_A \rho |\boldsymbol{V}|^2 \, dA dx \tag{25}$$

where ρ is the density of the micro-beam, and according to Pai, Qian, and Du (2013)), the velocity of a Rayleigh beam spinning about its elastic axis is:

$$\boldsymbol{V} = (\dot{u} - \Omega z)\boldsymbol{i} + \left[-x\left(\dot{u}' + \Omega w'\right) - z(\dot{w}' - \Omega u')\right]\boldsymbol{j} + (\dot{w} + \Omega x)\boldsymbol{k} \tag{26}$$

2.3. Variational formulation via the extended Hamilton's principle

The extended Hamilton's principle stipulates that the true dynamic trajectory of the system's motion between the time interval t_1 and t_2 is an extremum of the integral of the Lagrangian function $\left(\boldsymbol{\mathcal{L}} = \boldsymbol{\Pi}_K - \boldsymbol{\Pi}_S\right)$. That is (Reddy, 2002):

$$I = \int_{t_1}^{t_2} \left(\Pi_K - \Pi_S\right) dt \tag{27}$$

Plugging Equations (24)–(26) into Equation (27) yields the energy functional in the form $\boldsymbol{\mathcal{L}} = f(y, t, u, w, u_y, w_y, u_t, w_t, u_{yy}, w_{yy}, u_{ty}, w_{ty})$.

A necessary condition to make the integral stationary is to assume the following family of trial functions for the field variables:

$$\bar{u}(y,t) = u(y,t) + \in \eta(y,t); \tag{28a}$$

$$\bar{w}(y,t) = w(y,t) + \in \eta(y,t) \tag{28b}$$

and then enforce

$$\left.\frac{\partial \bar{I}}{\partial \in}\right|_{\in=0} = 0; \quad \mathcal{L} = f(y,\ t,\ \bar{u},\ \bar{w},\ \bar{u}_y,\ \bar{w}_y,\ \bar{u}_t,\ \bar{w}_t,\ \bar{u}_{yy},\ \bar{w}_{yy},\ \bar{u}_{ty},\ \bar{w}_{ty}) \tag{29a, b}$$

where both $\bar{u}$ and $\bar{w}$ represent the so-called variations in the original state variables, while $\in$ is a small parameter and η is a member of (at least) twice differentiable continuous functions. By using Equation (29b) in the differentiated integral resulting from Equation (27), a series of integration by parts is carried out and at the end of the differentiations, one sets $\in$ to zero and then replaces all occurrences of $(\bar{u},\ \bar{w},\ \bar{u}_y,\ \bar{w}_y,\ \bar{u}_t,\ \bar{w}_t,\ \bar{u}_{yy},\ \bar{w}_{yy},\ \bar{u}_{ty},\ \bar{w}_{ty})$ by $(u, w, u_y, w_y, u_t, w_t, u_{yy}, w_{yy}, u_{ty}, w_{ty})$ to retrieve the coupled Euler–Lagrange equations of the system as:

$$\frac{\partial f}{\partial u} - \frac{d}{dy}\frac{\partial f}{\partial u_y} - \frac{d}{dt}\frac{\partial f}{\partial u_t} + \frac{d^2}{dy^2}\frac{\partial^2 f}{\partial u_{yy}} + \frac{d^2}{dtdy}\frac{\partial^2 f}{\partial u_{yt}} = 0 \tag{30}$$

$$\frac{\partial f}{\partial w} - \frac{d}{dy}\frac{\partial f}{\partial w_y} - \frac{d}{dt}\frac{\partial f}{\partial w_t} + \frac{d^2}{dy^2}\frac{\partial^2 f}{\partial w_{yy}} + \frac{d^2}{dtdy}\frac{\partial^2 f}{\partial w_{yt}} = 0 \tag{31}$$

Further, replacing the function f in Equations (30) and (31) with the expressions generated by the difference of the expressions for the kinetic and total potential energy (i.e. $\Pi_K - \Pi_S$), one obtains the equations of motion of the spinning pre-twisted micro-structured Rayleigh beam as:

$$\begin{aligned} &\mathrm{A}_1 u + \mathrm{A}_2 \dot{w} + \mathrm{A}_3 \ddot{u} + \mathrm{A}_4 w' + \mathrm{A}_5 \dot{u}' + \mathrm{A}_6 \ddot{w}' + \mathrm{A}_7 u'' \\ &+ \mathrm{A}_8 \dot{w}'' + \mathrm{A}_9 \ddot{u}'' + \mathrm{A}_{10} w''' + \mathrm{A}_{11} u'''' = 0 \end{aligned} \tag{32}$$

$$\begin{aligned} &B_1 w + B_2 \dot{u} + B_3 \ddot{w} + \mathrm{B}_4 u' + \mathrm{B}_5 \dot{w}' + \mathrm{B}_6 \ddot{u}' \\ &+ \mathrm{B}_7 w'' + \mathrm{B}_8 \dot{u}'' + \mathrm{B}_9 \ddot{w}'' + \mathrm{B}_{10} u''' + \mathrm{B}_{11} w'''' = 0 \end{aligned} \tag{33}$$

For the sake of clarity, the coefficients $A_1 - A_{11}$ and $B_1 - B_{11}$ are provided in Table 1. In order to solve the differential equations representing the motions of the spinning pre-twisted microstructured Rayleigh beam, the scale-dependent Dirichlet boundary conditions that must be supplemented with these equations are:

$$\begin{aligned} V_X = {} & I_{XX}\rho(-\gamma\Omega^2 w - \gamma\Omega\dot{u} - \Omega^2 u' + \Omega\dot{w}') + I_{ZZ}\rho(-\gamma\Omega\dot{u} + \gamma\ddot{w} + \Omega\dot{w}' + \ddot{u}') \\ &+ EI_{XX}(2\gamma^3 w + 4\gamma^2 u' - 2\gamma w'') + AG\ell^2(2\gamma^3 w + 5\gamma^2 u' - 4\gamma w'' - u''') \\ &+ \mathrm{EI}_{ZZ}(\gamma^2 u' - 2\gamma w'' - u''') \end{aligned} \tag{34}$$

Table 1. The coefficients and their expressions for the governing equations (Equations 32 and 33).

Coefficients	Expressions
A_1	$-EI_{ZZ}\gamma^4 - AG\ell^2\gamma^4 + I_{ZZ}\gamma^2\rho\Omega^2$
A_2	$-(I_{XX} + I_{ZZ})\gamma^2\rho\Omega$
A_3	$-(A + I_{XX}\gamma^2)\rho$
A_4	$\gamma(2E(I_{XX} + I_{ZZ})\gamma^2 + 4AG\ell^2\gamma^2 - (I_{XX} + I_{ZZ})\rho\Omega^2)$
A_5	$-2(I_{XX} + I_{ZZ})\gamma\rho\Omega$
A_6	$(I_{XX} + I_{ZZ})\gamma\rho$
A_7	$2E(2I_{XX} + I_{ZZ})\gamma^2 + 6AG\ell^2\gamma^2 - I_{XX}\rho\Omega^2$
A_8	$(I_{XX} + I_{ZZ})\rho\Omega$
A_9	$I_{ZZ}\rho$
A_{10}	$-2(E(I_{XX} + I_{ZZ}) + 2AG\ell^2)\gamma$
A_{11}	$-EI_{ZZ} - AG\ell^2$
B_1	$-EI_{XX}\gamma^4 - AG\ell^2\gamma^4 + I_{XX}\gamma^2\rho\Omega^2$
B_2	$(I_{XX} + I_{ZZ})\gamma^2\rho\Omega$
B_3	$-(A + I_{ZZ}\gamma^2)\rho$
B_4	$-2E(I_{XX} + I_{ZZ})\gamma^3 - 4AG\ell^2\gamma^3 + (I_{XX} + I_{ZZ})\gamma\rho\Omega^2$
B_5	$-2(I_{XX} + I_{ZZ})\gamma\rho\Omega$
B_6	$-(I_{XX} + I_{ZZ})\gamma\rho$
B_7	$2E(I_{XX} + 2I_{ZZ})\gamma^2 + 6AG\ell^2\gamma^2 - I_{ZZ}\rho\Omega^2$
B_8	$-(I_{XX} + I_{ZZ})\rho\Omega$
B_9	$I_{XX}\rho$
B_{10}	$2(E(I_{XX} + I_{ZZ}) + 2AG\ell^2)\gamma$
B_{11}	$-EI_{XX} - AG\ell^2$

$$\begin{aligned} V_Z = {} & \mathrm{I}_{ZZ}\rho(\gamma\Omega^2 u - \gamma\Omega\dot{w} - \Omega^2 w' - \Omega\dot{u}') \\ & + I_{XX}\rho(-\gamma\Omega\dot{w} - \gamma u'' - \Omega\dot{u}' + \ddot{w}') \\ & + \mathrm{EI}_{ZZ}(-2\gamma^3 u + 4\gamma^2 w' + 2\gamma u'') + \mathrm{EI}_{XX}(\gamma^2 w' + 2\gamma u'' - w''') \\ & + AG\ell^2(-2\gamma^3 u + 5\gamma^2 w' + 4\gamma u'' - w''') \end{aligned} \tag{35}$$

$$M_{XX} = -EI_{XX}\left(-w\gamma^2 - 2\gamma u' + w''\right) - AG\ell^2(-w\gamma^2 - 2\gamma u' + w'') \tag{36}$$

$$M_{ZZ} = EI_{ZZ}(-u\gamma^2 + 2\gamma w' + u'') + AG\ell^2(-u\gamma^2 + 2\gamma w' + u'') \tag{37}$$

The following geometric properties have been employed in Table 1:

$$I_{XX} = \int_{-\frac{b}{2}}^{\frac{b}{2}}\int_{-\frac{h}{2}}^{\frac{h}{2}} z^2 dzdx; I_{ZZ} = \int_{-\frac{b}{2}}^{\frac{b}{2}}\int_{-\frac{h}{2}}^{\frac{h}{2}} x^2 dxdz; A = \int_{-\frac{b}{2}}^{\frac{b}{2}}\int_{-\frac{h}{2}}^{\frac{h}{2}} dxdz \tag{38a, b, c}$$

It is noted that the derived governing equations reduce to a number of mathematical models reported in the literature, but two of these are of interest. For instance, if in Equations (32) and (33) one allows $\ell = 0$, $\Omega = 0$, $\rho I_{XX} = \rho I_{ZZ} = 0$, then the model of the classical non-spinning pre-twisted Euler–Bernoulli beam, reported by Banerjee (2001)), is obtained as:

$$\begin{aligned} & A\rho\ddot{u} + EI_{XX}\left(-2\gamma^3 w' - 4\gamma^2 u'' + 2\gamma w'''\right) \\ & + E\,I_{ZZ}\left(u\gamma^4 - 2\gamma^3 w' - 2\gamma^2 u'' + 2\gamma w''' + u''''\right) = 0 \end{aligned} \tag{39}$$

$$\begin{aligned} & A\rho\ddot{w} + EI_{ZZ}\left(2\gamma^3 u' - 4\gamma^2 w'' - 2\gamma u'''\right) \\ & + EI_{XX}\left(w\gamma^4 + 2\gamma^3 u' - 2\gamma^2 w'' - 2\gamma u''' + w''''\right) = 0 \end{aligned} \tag{40}$$

Next, if one assumes that $I_{XX} = I_{ZZ} = I, \gamma = 0,\ \ell = 0$, then the reported model of spinning Rayleigh beam developed by Pai et al. (2013) is obtained (as shown in Equations (41) and (42)).

$$A\rho\ddot{u} + I\rho\left(\Omega^2 u'' - 2\Omega\dot{w}'' - \ddot{u}''\right) + \mathrm{EI}\,u'''' = 0 \tag{41}$$

$$A\rho\ddot{w} + I\rho\left(\Omega^2 w'' + 2\Omega\dot{u}'' - \ddot{w}''\right) + EI\,w'''' = 0 \tag{42}$$

3. Wave propagation study

We study the nature of the spectrum and dispersion relations as well as phase speed/ group velocity of the waves within this system by using Equations (32) and

(33). For a start, the following exponential functions are employed to examine the characteristics of the wave within the system:

$$\left\{ \begin{array}{c} u(y,t) \\ w(y,t) \end{array} \right\} = \left\{ \begin{array}{c} U(y,\omega) \\ W(y,\omega) \end{array} \right\} e^{-i(Ky-\omega t)} \tag{43}$$

where $U(y,\omega)$ and $W(y,\omega)$ are the spectral amplitudes of the propagating waves. Besides, $i = \sqrt{-1}$, while K is the wavenumbers (typically real and positive, and representing the number of complete waves in length 2π). Further, ω denotes the radial frequency of the wave, and it is associated with the cyclic frequency (f) by the relation $2\pi f$. Plugging Equations (43) into Equations (34) and (35), one obtains the following matrix equation:

$$\left[\begin{array}{cc} a_{11} & a_{12} \\ a_{21} & a_{22} \end{array} \right] \left\{ \begin{array}{c} U \\ W \end{array} \right\} = \left\{ \begin{array}{c} 0 \\ 0 \end{array} \right\} \tag{44}$$

For mathematical convenience, we re-scale the dimensionality of the problem by introducing the following normalising parameters:

$$\begin{aligned} &\xi = \frac{y}{L};\ \alpha = I_{XX}/I_{ZZ};\ \lambda^2 = \omega^2 \rho A L^4/EI_{ZZ};\ \eta^2 = \Omega^2/\omega^2; \\ &\beta = \ell/h;\ r^2 = \frac{I_{ZZ}}{A\,L^2};\ \psi = \gamma L;\ G = \frac{E}{2(1-\nu)};\ k = KL \end{aligned} \tag{45}$$

With the help of the normalising parameters defined in Equation (45), the elements of the matrix a_{ij} in Equation (44) are obtained as:

$$a_{11} = \left[\begin{array}{c} -\lambda^2 + k^4\left(1 + \frac{6\beta^2}{1+\upsilon}\right) - r^2\alpha\lambda^2\psi^2 - r^2\eta^2\lambda^2\psi^2 + \psi^4 + \frac{6\beta^2\psi^4}{1+\upsilon} + k(2r^2\eta\lambda^2\psi \\ +2r^2\alpha\eta\lambda^2\psi) + k^2\left(-r^2\lambda^2 - r^2\alpha\eta^2\lambda^2 + 2\psi^2 + 4\alpha\psi^2 + \frac{36\beta^2\psi^2}{1+\upsilon}\right) \end{array} \right] \tag{46a}$$

$$a_{12} = \left[\begin{array}{c} k^2\left(\mathrm{i}r^2\eta\lambda^2 + \mathrm{i}r^2\alpha\eta\lambda^2\right) + \mathrm{i}r^2\eta\lambda^2\psi^2 + \mathrm{i}r^2\alpha\eta\lambda^2\psi^2 + k^3\left(2\mathrm{i}\psi + 2\mathrm{i}\alpha\psi + \frac{24\mathrm{i}\beta^2\psi}{1+\upsilon}\right) \\ +k\left(-\mathrm{i}r^2\lambda^2\psi - \mathrm{i}r^2\alpha\lambda^2\psi - \mathrm{i}r^2\eta^2\lambda^2\psi - \mathrm{i}r^2\alpha\eta^2\lambda^2\psi + 2\mathrm{i}\psi^3 + 2\mathrm{i}\alpha\psi^3 + \frac{24\mathrm{i}\beta^2\psi^3}{1+\upsilon}\right) \end{array} \right] \tag{46b}$$

$$a_{21} = \left[\begin{array}{c} k^2\left(-\mathrm{i}r^2\eta\lambda^2 - \mathrm{i}r^2\alpha\eta\lambda^2\right) - \mathrm{i}r^2\eta\lambda^2\psi^2 - \mathrm{i}r^2\alpha\eta\lambda^2\psi^2 + k^3\left(-2\mathrm{i}\psi - 2\mathrm{i}\alpha\psi - \frac{24\mathrm{i}\beta^2\psi}{1+\upsilon}\right) \\ +k\left(\mathrm{i}r^2\lambda^2\psi + \mathrm{i}r^2\alpha\lambda^2\psi + \mathrm{i}r^2\eta^2\lambda^2\psi + \mathrm{i}r^2\alpha\eta^2\lambda^2\psi - 2\mathrm{i}\psi^3 - 2\mathrm{i}\alpha\psi^3 - \frac{24\mathrm{i}\beta^2\psi^3}{1+\upsilon}\right) \end{array} \right] \tag{46c}$$

$$a_{22} = \left[\begin{array}{c} -\lambda^2 + k^4\left(\alpha + \frac{6\beta^2}{1+\upsilon}\right) - r^2\lambda^2\psi^2 - r^2\alpha\eta^2\lambda^2\psi^2 + \alpha\psi^4 + \frac{6\beta^2\psi^4}{1+\upsilon} + k(2r^2\eta\lambda^2\psi \\ + 2r^2\alpha\eta\lambda^2\psi) + k^2\left(-r^2\alpha\lambda^2 - r^2\eta^2\lambda^2 + 4\psi^2 + 2\alpha\psi^2 + \frac{36\beta^2\psi^2}{1+\upsilon}\right) \end{array} \right] \tag{46d}$$

The elements of the matrix a_{ij} contain the non-dimensional wavenumber (k), the rotary inertia parameter (r), the frequency parameter (λ), the spinning parameter (η), the normalised material length-scale parameter (β) as well as α (which is essentially the rigidity ratio). For non-trivial solutions, the determinant of a_{ij} is set to zero as:

$$\begin{vmatrix} a_{11} & a_{12} \\ a_{21} & a_{22} \end{vmatrix} = 0 \tag{47}$$

The following octic characteristic relation is obtained from the determinant in Equation (47):

$$C_1k^8 + C_2k^6 + C_3k^5 + C_4k^4 + C_5k^3 + C_6k^2 + C_7k^1 + C_8k^0 = 0 \tag{48}$$

The coefficients $\left(C_1 - C_8\right)$ of the characteristic relation have been relegated to the Appendix. We note here that if the spinning parameter (η) is eliminated, the odd powers of the non-dimensional wavenumber (i.e. k^5, k^3 and k^1) disappear from the characteristic relation. Consequently, one may then apply the order reduction method, expounded in Abramowitz and Stegun (Abramowitz & Stegun, 1965), to shrink the octic characteristic relation to its quartic equivalent (the root of which is amenable to a closed-form solution). In the meantime, it is observed that a sufficiently simpler characteristic relation can be obtained if we exclude r along with β, υ and η from the coefficients of Equation (48) (as demonstrated in Equation (49)).

$$\begin{array}{l} k^8\alpha - 4k^6\alpha\psi^2 + k^4(-\lambda^2 - \alpha\lambda^2 + 6\alpha\psi^4) + k^2(-6\lambda^2\psi^2 - 6\alpha\lambda^2\psi^2 - 4\alpha\psi^6) \\ + \alpha\psi^8 - \lambda^2\psi^4 - \alpha\lambda^2\psi^4 + \lambda^4 = 0 \end{array} \tag{49}$$

3.1. Cut-off frequencies of the propagating waves

This section highlights the low-frequency long-wavelength limits of the wave patterns arising from the full model. In principal, the low-frequency, long-wavelength limit of the wave is obtained when we allow $k \to 0$, and this typically reveals the so-called cut-off frequency of elastic waveguides. Table 2 highlights the expressions for the non-zero cut-off frequencies of the propagating waves predicted from the full model and three different reduced models. The full model is shown in row 1, and it is based on Equation (48). Alongside the full model are three degenerate models: (i) reduced model I, which represents a non-spinning pre-twisted Rayleigh micro-scale beam; (ii) reduced model II, which characterises a

Table 2. The cut-off frequencies of the propagating waves.

	Models	Cut-off frequencies
1	Full model of the pre-twisted spinning micro-scale Rayleigh beam^{++}	$\lambda_{c1} = \sqrt{\frac{P_1}{2P_2} - \frac{\sqrt{P_1^2-4P_2P_3}}{2P_2}}; \lambda_{c2} = \sqrt{\frac{P_1}{2P_2} + \frac{\sqrt{P_1^2-4P_2P_3}}{2P_2}}$
2	Reduced model I	$\lambda_{c1} = \frac{\mathrm{i}\sqrt{\alpha+6\beta^2+\alpha\upsilon\psi^2}}{\sqrt{-(1+\upsilon)(1+r^2\psi^2)}}; \lambda_{c2} = \frac{\mathrm{i}\sqrt{1+6\beta^2+\upsilon\psi^2}}{\sqrt{-(1+\upsilon)(1+r^2\alpha\psi^2)}}$
3	Reduced model II	$\lambda_{c1} = \frac{\sqrt{\alpha}\psi^2}{\sqrt{1+r^2\psi^2}}; \lambda_{c2} = \frac{\psi^2}{\sqrt{1+r^2\alpha\psi^2}}$
4	Reduced model III	$\lambda_{c1} = \psi^2; \lambda_{c2} = \sqrt{\alpha}\psi^2$

$^{++}$The $P_i (i = 1, 2, 3)$ in row 1 are provided in Equations (51)–(53).

non-spinning pre-twisted Rayleigh with no scale-dependent property; and (iii) reduced model III, which idealises a pre-twisted beam without the trio of rotary inertia, small-scale effect and the spinning rate. From Table 2, it is noticed that the cut-off frequencies for the full model are strongly influenced by the small-scale parameter, the angle of twist and the spinning rate. Further, two non-zero cut-off frequencis, attributable to the existence of the coupled wave fields in the system, are obtained for each of the models (designated with λ_{c1} and λ_{c2}).

$$P_1 = (1+\upsilon)\psi^4(r^2\alpha^2(1+\upsilon)\psi^2 + (1+\upsilon)(1+r^2\psi^2) + 6\beta^2(2+r^2(1+\eta^2)\psi^2) + \alpha(1+\upsilon+2r^2(\eta^2+3\beta^2(1+\eta^2))\psi^2 + 2r^2\eta^2\upsilon\psi^2)) \tag{51}$$

$$P_2 = (1+\upsilon)^2(1+r^2(1+\alpha)(1+\eta^2)\psi^2 + r^4\alpha(-1+\eta^2)^2\psi^4) \tag{52}$$

$$P_3 = (1+6\beta^2+\upsilon)(\alpha+6\beta^2+\alpha\upsilon)\psi^8 \tag{53}$$

3.2. Spectrum patterns

Solving the characteristics equation (Equation (48)) yields a map of the pattern of relationships between the wavenumbers and the frequencies of the propagating elastic waves. Bearing in mind the Abel–Ruffini theorem (Prasolov, 2009), it is noted that an analytical closed-form solution for the characteristics equation may not be possible due to the order of the polynomial (order is greater than five). It is therefore necessary to resort to the use of numerical analysis in order to make sense of the role of the geometric, process and material parameters on the nature of the propagating waves dictated by the octic characteristics equation. For numerical analyses, a set of realistic values for the dimensionless parameters defined in Equation (45) is obtained by using the following properties of a typical micro-scale pre-twisted beam (Gong, Ehmann, & Lin, 2003): $E = 650$ GPa; $G = 250$ GPa; $\rho = 15$ g/cm^3; $h = 457$ μm; $L = 8.89$ mm; $A = 5.2 \times 10^{-2}$ mm^2; $I_{ZZ} = 8.28 \times 10^{-4}$ mm^4; $I_{XX} = 9.06 \times 10^{-5}$ mm^4.

Using the aforementioned properties, the evolution of the frequency spectrum curves for the wave modes is displayed in Figures 3–7. Figure 3 shows the plots of the complex spectrum relation solved numerically with

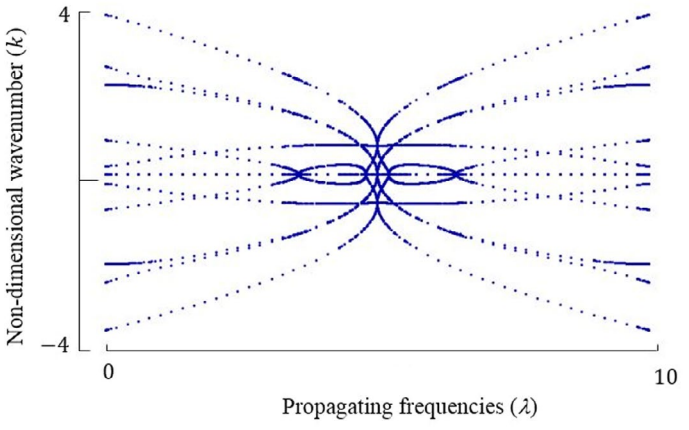

Figure 3. A plot of the spectrum relations, considering both imaginary and real components of the forward and backward moving waves within the pre-twisted micro-scale Rayleigh beam.

$\psi = \pi/2$; $\alpha = 0.109$; $\beta = 0.1$; $\upsilon = 0.25$; $\eta = 1$; $r = 0.014$. This figure is an amalgam of the evanescent and propagating forward and backward waves derived from the spectrum relation, which according to Chin (2014) represents the entire physical account of wave propagating within an elastic system. In the meantime, it is noted that propagating wave modes are most relevant to high-frequency vibration and quasi-static stability, while the evanescent waves are typically energy trapping non-propagating waves (Karp & Durban, 2005). For this reason, the rest of the paper focuses on the propagating waves.

Figure 4 illustrates the evolution of the spectrum curves for varying values of the pre-twist angle. Other parameters, based on the properties defined earlier, are kept as $\alpha = 0.109$; $\beta = 0.1$; $\upsilon = 0.25$; $\eta = 1$; $r = 0.014$. Figure 4(a)–(c) are the spectrum curves from the full model. Figure 4(d) is a check on the accuracy of the solution scheme, obtained by recovering the quasi-static results for a beam with no pre-twist presented in Doyle (1997). Some general observations deduced from these plots are as follows. First, the presence of pre-twist angle introduces bifurcation points that appear to split the elastic waves within the system. For very small pre-twist angles, the bifurcation point almost coincides with the origin. Moreover, the frequency at which the bifurcation points occur shift in the positive direction with increasing values of the pre-twist angle (as seen in Figure 4(a)–(c)). Second, for large values of pre-twist angle, the branches of the propagating wave increase from 2 to 3, in the low-frequency range. Third, the propagating waves are dispersive, (that is, there is a noticeable change in the spatial periods of the waves with a change in frequency). Figure 5 demonstrates the influence of rotary inertia on the spectrum curves at a fixed angle of twist, while Figure 5(b) shows the variation of the spectrum curves with changes in the values of the small-scale parameter at a fixed angle of twist. From these figures, it is noticed that the frequency at which the bifurcation point occurs shifts forward with increasing values of the small-scale parameter, but it pulls back as the rotary inertia is increased.

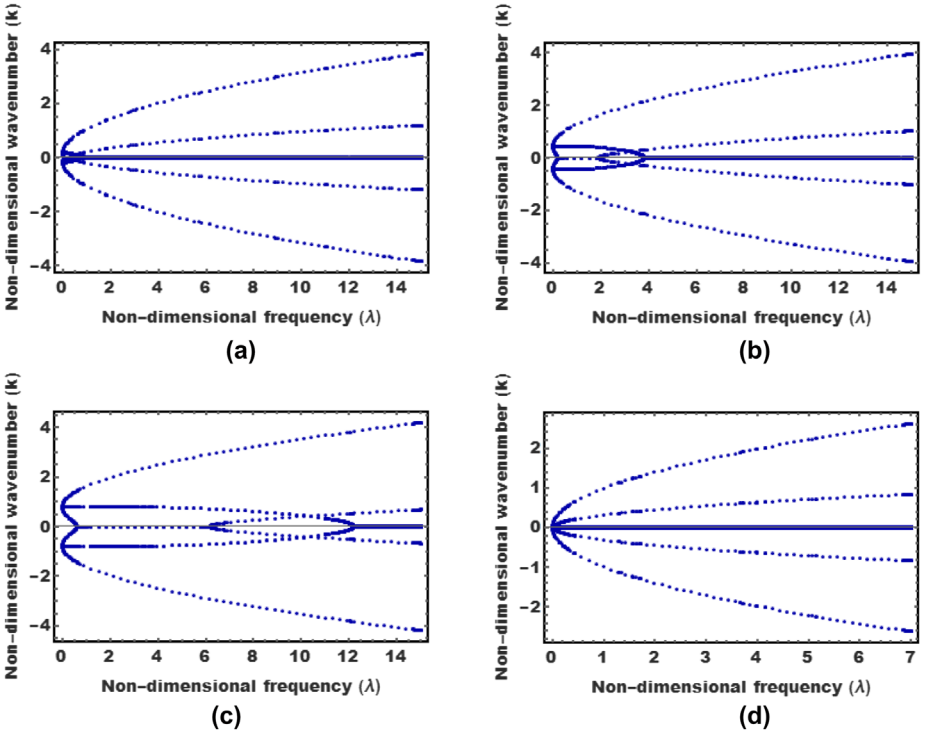

Figure 4. Wavenumber as a function of angle of twist: (a) $\psi = \pi/18$; (b) $\psi = 5\pi/36$; (c) $\psi = \pi/4$; and (d) $\psi = 0$.

Figure 6 highlights the influence of flexural rigidity ratio (α) on the spectrum relations. Here, the flexural rigidity ratio is varied while the other parameters are kept constant ($\psi = \pi/4$; $\beta = 0.1$; $\upsilon = 0.25$; $\eta = 1$; $r = 0.014$). For this plot, the variation of the rigidity ratio is set, following Leung and Fan (2010), within a practical range (i.e. $\alpha = 1, 0.683, 0.260, 0.109$). For validation, Figure 6(a) is a special case of a beam with $\alpha = 1$ and zero pre-twist angle (i.e. $\psi = 0$), which essentially is a square cross-sectioned non-pre-twisted beam with a scale-dependent property, and it is seen from this that the propagating waves collapsed into a single wave mode that aligns with the behaviour predicted by Doyle (Doyle, 1997). Further inspections of Figure 6(b)–(d) show that lower values of the rigidity ratio lead to increment of the wavelength of one of the flexural wave modes (the upper branch). Moreover, Figure 6(d) (which has the lowest α) reveals that the spectrum plot assumes a pattern similar in behaviour to what occurs at moderately high values of the pre-twist angle (shown in Figure 4). That is, the occurrence of two very dispersive waves along with a third fast-decaying low-wavelength branch.

Figures 7–9 are the three-dimensional representation of the spectrum relations. An examination of these figures indicates the decreasing value of the wavenumber as both angle of twist and small-scale parameter increases. In all, the curves here are provided in terms of normalised propagating frequency and non-dimensional

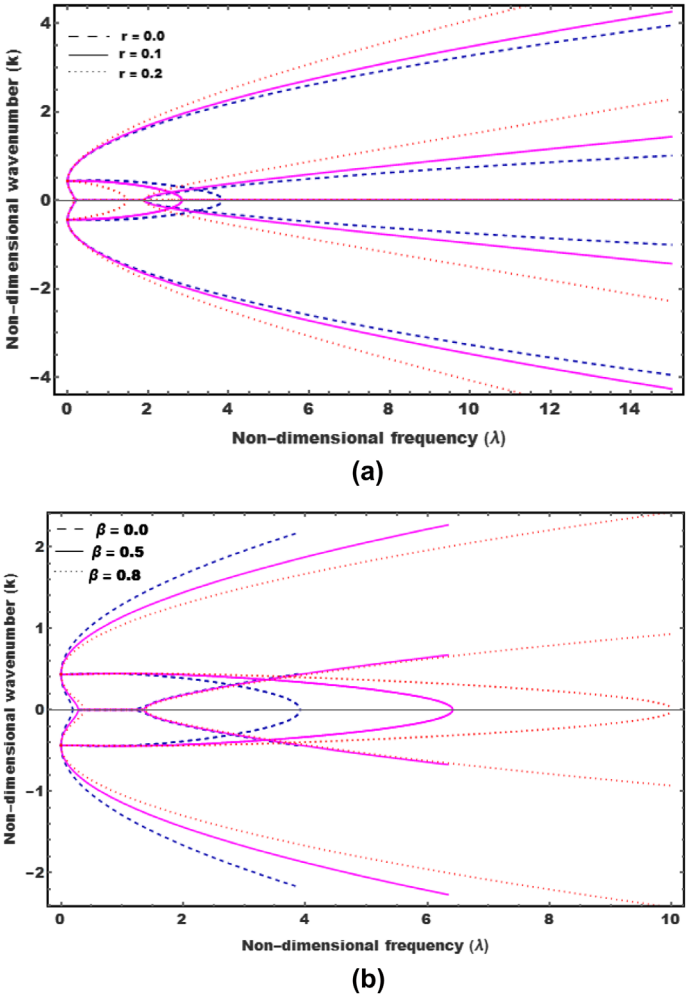

Figure 5. (a) Influence of rotary inertia on the spectrum curves at a fixed angle of twist; (b) influence of small-scale parameter on the spectrum curves at a fixed angle of twist.

wavenumber. Furthermore, these plots are meant to supplement Figures 4 and 6 by presenting the three-dimensional relationship between the wavenumber, frequency and: (a) the angle of twist (Figure 7); (b) the small-scale effect (Figure 8); (c) the spinning parameter (Figure 9).

3.3. *Influence of model's parameter on speeds of propagating waves*

The propagation of a wave pulse in a medium is governed by the phase speeds (speed of propagation of the waveform) and the group velocity (speed at which the envelope of a group of waves propagates). The determination of the phase speed (C_p) and group speed (C_g) follows from:

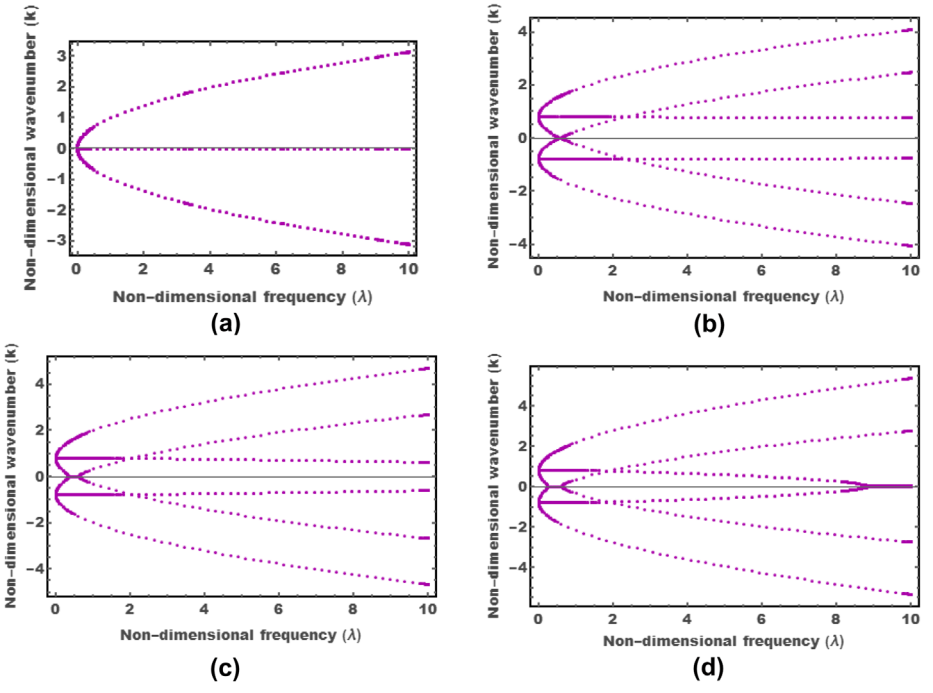

Figure 6. Wavenumber as a function of rigidity ratio; (a)$\alpha = 1; \psi = 0$; (b) $\alpha = 0.638; \psi = \pi/4$; (c) $\alpha = 0.260; \psi = \pi/4$; (d) \alpha = 0.109; \psi = \pi /4.

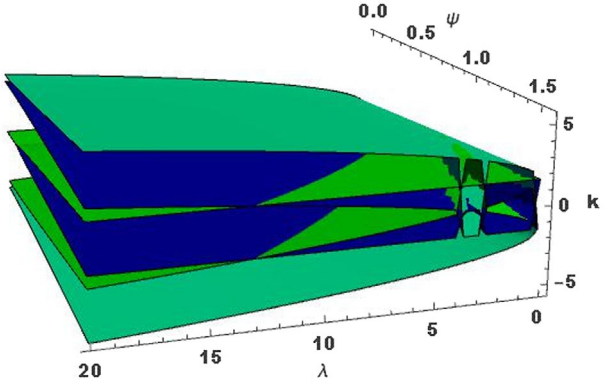

Figure 7. Variation of the wavenumber with the angle of twist and the propagating frequencies.

$$C_p = \text{Real}\left(\frac{\lambda}{k}\right) \tag{54}$$

$$C_g = \frac{\partial \lambda}{\partial k} \tag{55}$$

where use has been made of the parameters defined in Equation (45). To determine C_p and C_g, we return to Equation (48) and obtain a quartic characteristic equation in terms of λ as:

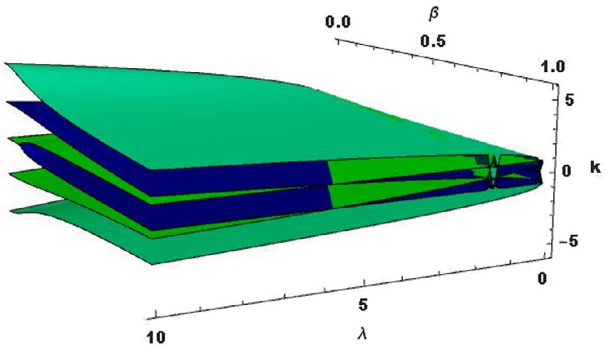

Figure 8. Variation of the wavenumber with the small-scale effect parameter and the propagating frequencies.

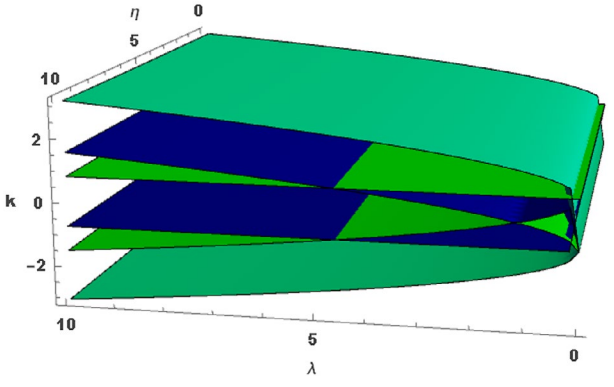

Figure 9. Variation of the wavenumber with the spinning rate and the propagating frequencies.

$$\lambda^4 Q_1 - \lambda^2 Q_2 + Q_3 = 0 \tag{56}$$

The closed-form solutions for Equation (56) then take the form:

$$\lambda_{1,2} = \pm\sqrt{\frac{Q_2 - \sqrt{Q_2^2 - 4Q_1Q_3}}{2Q_1}}; \quad \lambda_{3,4} = \pm\sqrt{\frac{Q_2 + \sqrt{Q_2^2 - 4Q_1Q_3}}{2Q_1}} \tag{57a, b}$$

where $Q_k (k = 1, 2, 3)$ are provided in Appendix 1. Equation (57) defines the relationship between the frequency parameter and the wavenumbers. However, as underscored in Equation (54), a division of these expressions by the real components of the wavenumbers gives C_p. The group velocities are then eventually determined by noting that:

$$C_g = C_p + k\frac{dC_p}{dk} = \frac{C_p}{1 - \frac{\lambda}{C_p}\frac{dC_p}{d\lambda}} \tag{58}$$

Figures 10–13 illustrates the sensitivity of the phase speed and group velocity of the coupled waves to changes in the model's parameter. Specifically, Figure 10 depicts the variation of the relationship between the phase speeds and wavenumber (the dispersion relation) for various values of the small-scale parameter. Each of Figure 10(a)–(d) shows four branches; two branches for each angle of twist considered (i.e. $\psi = \pi/18$ and $\pi/4$). Besides, the two branches generated for a single value of the angle of twist represent the phase speeds of the flexural elastic wave in the two orthogonal planes of deformation. Figure 10(a) represents the prediction from the classical theory ($\upsilon = 0, \beta = 0$) which, as can be observed, predicts a low-speed propagating waves. In contrast, by considering the scale-dependent property, one notices that the wave speed increases gradually with increasing value of the small-scale parameter as shown in Figure 10(b)–(d). A further examination of Figure 10(d) shows that as the small-scale parameter approaches the height of the cross section of the ultra-thin beam ($\beta = 0.8$), the magnitude of the phase speed becomes more than double the value predicted by the classical theory.

Figure 11 depicts, in a three-dimensional relationship, the sensitivity of the dispersion relation to changes in the value of the angle of twist, small-scale parameter and the spinning rate. It is noticed from Figure 11(a) that when the pre-twist angle is small (e.g. $\psi = \pi/18$), the phase speeds of the coupled waves approach each other (this is reflected by the red plot). However, increasing the twisting of

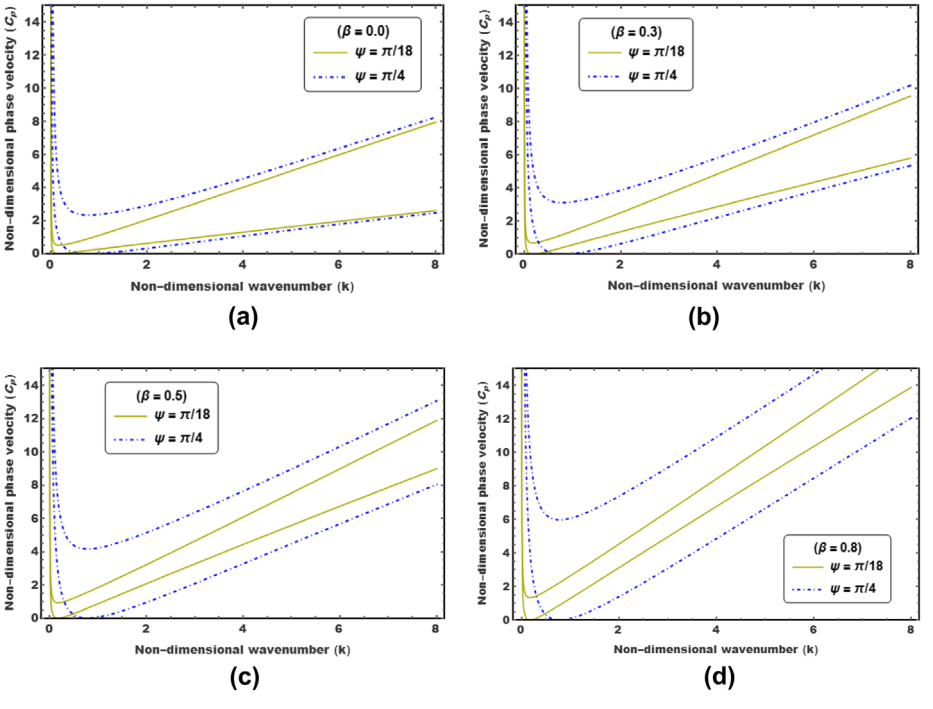

Figure 10. Variation of the phase speed for various values of the small-scale parameter and angle of twist.

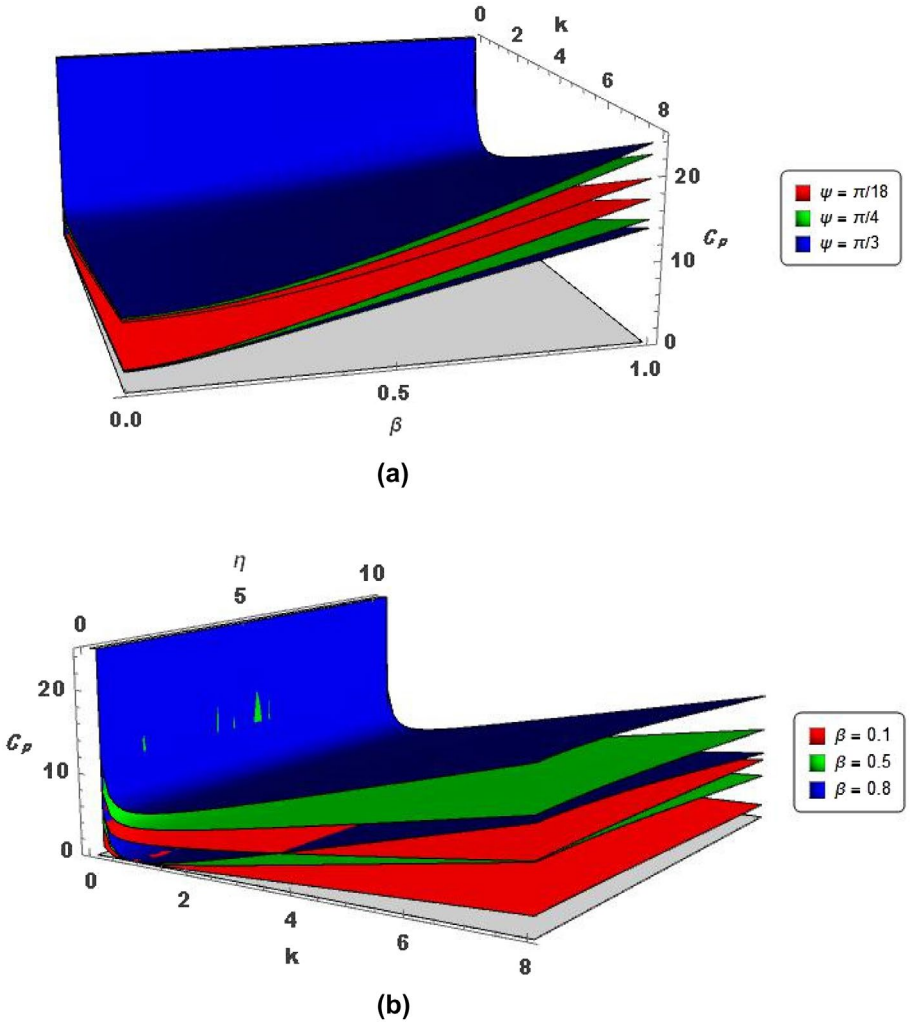

Figure 11. Sensitivity of the phase speed dispersion with: (a) small-scale parameter for different values of angle of twist; (b) spinning rate for different values of small-scale parameter.

the cross section increases (decreases) the phase speed of the wave in the plane with higher (lower) moment of inertia.

Figures 12 and 13 represent the group velocity equivalent of the parametric studies presented in Figures 10 and 11. The group velocity–wavenumber relationship bears a similarity with the phase speed–wavenumber plots in terms of the occurrence of two branches. However, there is a bit of difference that needs to be pointed out. First, for the case when $\beta = 0$ (classical theory shown in Figure 12(a)), the two branches of the group velocity are clearly delineated. However, the gap between these two branches shrinks as the material length-scale parameter approaches the height of the cross section of the ultra-thin beam ($\beta = 0.8$). In addition, the group velocity increases as the material length-scale parameter approaches the height of the cross-section of the ultra-thin beam. Figure 13

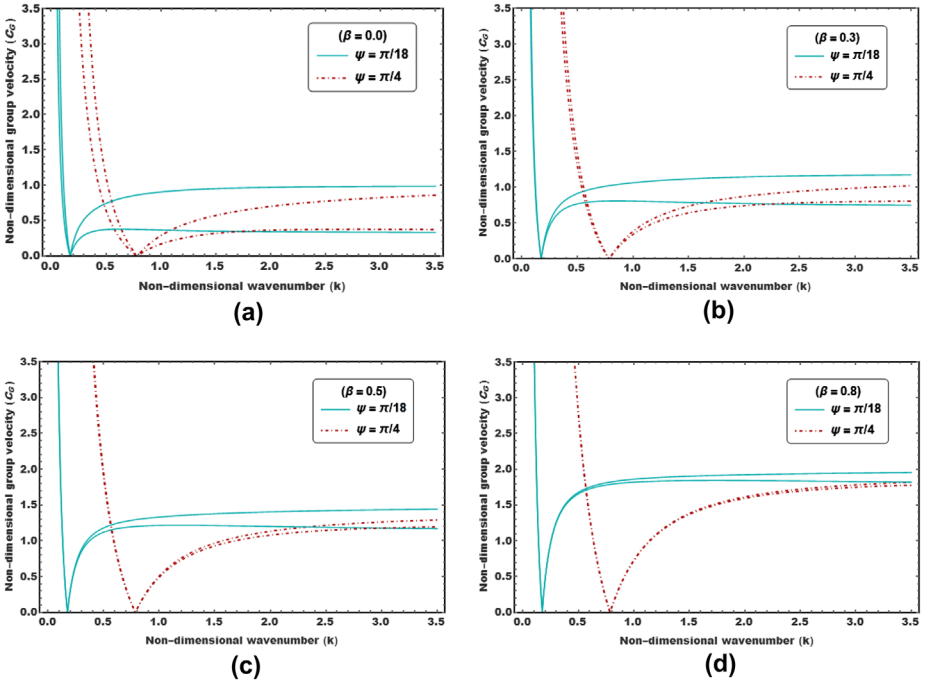

Figure 12. The variation of the group velocity for various values of the small-scale parameter and angle of twist.

highlights the sensitivity of group velocity dispersion relation with: (i) the small-scale parameter for different values of angle of twist (Figure 13(a)); and (ii) the spinning rate for different value of the small-scale parameter (Figure 12(b)). From these plots, it is noticed that, the group velocity, just as the phase speed is not significantly affected by the spinning rate as compared to the influence of the angle of twist and the small-scale parameter introduced by the use of MCST.

4. Free vibration behaviour

In this section, the influence of the model's parameters on the resonant frequencies of the system is investigated. For the vibration behaviour, solution of the derived model is obtained by using the Rayleigh–Ritz method, and consideration is given to the effect of the small-scale parameter (β), rotary inertia (r), rigidity ratio (α) and spinning (η) on the natural frequencies of the pre-twisted Rayleigh microbeam. In general, the Rayleigh–Ritz method can handle various boundary conditions as enumerated in many studies (Ilanko, Monterrubio, & Mochida, 2015). For brevity sake, we studied the vibration behaviour of a cantilevered pre-twisted Rayleigh beam. Under this boundary condition, the shear forces and bending moments are zero at the free end, while the transverse displacements (u, w and slopes ($u'(y)$, $w'(y)$) are zero at the fixed end.

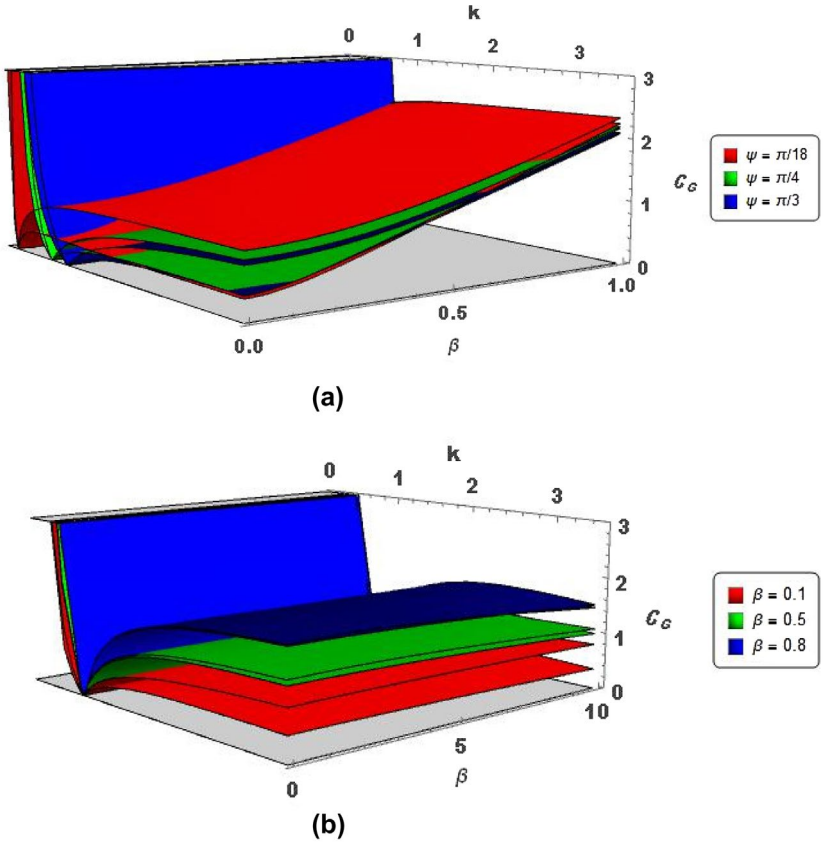

Figure 13. Sensitivity of group velocity dispersion with: (a) small-scale parameter for different values of angle of twist; (b) spinning rate for different values of small-scale parameter.

Written in the non-dimensional form, the general shear forces and bending moments for the spinning pre-twisted Rayleigh micro-beam with scale-dependent property takes the form:

$$\begin{aligned}\bar{V}_X = &-\mathrm{i}r^2(1+\alpha)\eta\lambda^2\psi U \\ &+ \frac{\psi(-r^2(1+\alpha\eta^2)\lambda^2(1+\upsilon)+2(\alpha+6\beta^2+\alpha\upsilon)\psi^2)}{1+\upsilon}W \\ &+ \frac{(-r^2(1+\alpha\eta^2)\lambda^2(1+\upsilon)+(1+30\beta^2+\upsilon+4\alpha(1+\upsilon))\psi^2)}{1+\upsilon}U' \\ &+ \mathrm{i}r^2(1+\alpha)\eta\lambda^2 W' - \frac{2(1+\alpha+12\beta^2+\upsilon+\alpha\upsilon)\psi}{1+\upsilon}W'' \\ &+ \left(-1-\frac{6\beta^2}{1+\upsilon}\right)U'''\end{aligned} \tag{59}$$

$$\begin{aligned}\bar{V}_Z = & \frac{\psi\left(r^2\left(\alpha+\eta^2\right)\lambda^2(1+\upsilon)-2\left(1+6\beta^2+\upsilon\right)\psi^2\right)}{1+\upsilon}U \\ & -\mathrm{i}r^2(1+\alpha)\eta\lambda^2\psi W-\mathrm{i}r^2(1+\alpha)\eta\lambda^2U' \\ & -\frac{\left(r^2\left(\alpha+\eta^2\right)\lambda^2(1+\upsilon)-\left(4+\alpha+30\beta^2+4\upsilon+\alpha\upsilon\right)\psi^2\right)}{1+\upsilon}W' \\ & +2\left(1+\alpha+\frac{12\beta^2}{1+\upsilon}\right)\psi U''+\left(-\alpha-\frac{6\beta^2}{1+\upsilon}\right)W'''\end{aligned} \tag{60}$$

$$\bar{M}_X = -\frac{(1+6\beta^2+\upsilon)}{1+\upsilon}(\psi^2U-2\psi W'-U'') \tag{61}$$

$$\bar{M}_Z = \frac{(\alpha+6\beta^2+\alpha\upsilon)}{1+\upsilon}(\psi^2W+2\psi U'-W'') \tag{62}$$

The simplified forms of Equations (59)–(62) compare with those in the literature. For instance, if the variables that relate to the scale-dependent property (i.e. β and υ), rotary inertia (r) and spinning rate are eliminated from these equations, the reduced expressions for the shear forces and bending moments of the classical model of pre-twisted Euler–Bernoulli beams is obtained as:

$$\bar{V}_X = 2\alpha\psi^3W+(1+4\alpha)\psi^2U'-2\psi W''-2\alpha\psi W''-U''' \tag{63}$$

$$\bar{V}_Z = -2\psi^3U+(4+\alpha)\psi^2W'+2\psi U''+2\alpha\psi U''-\alpha W''' \tag{64}$$

$$\bar{M}_X = \alpha(\psi^2W+2\psi U'-W'') \tag{65}$$

$$\bar{M}_Z = -\psi^2U+2\psi W'+U'' \tag{66}$$

Equations (63)–(66) match those reported by Banerjee (2001). Note that Banerjee (2001) employed k as the angle of twist per unit length. Moreover, if the parameters that define the scale-dependent property and the pre-twist angle (ψ) are also eliminated from Equations (59)–(62), one obtains the simplified expressions that match those reported by Pai et al. (2013) for the shear forces and bending moment of the spinning classical Rayleigh beam as:

$$\bar{V}_X = -r^2(1+\eta^2)\lambda^2U'+2\mathrm{i}r^2\eta\lambda^2W'-U''' \tag{67}$$

$$\bar{V}_Z = -2\mathrm{i}r^2\eta\lambda^2 U' - r^2\left(1+\eta^2\right)\lambda^2 W' - W''' \tag{68}$$

$$\bar{M}_X = -W'' \tag{69}$$

$$\bar{M}_Z = U''' \tag{70}$$

The transformed expressions for the strain and kinetic energies of the system required by the Rayleigh–Ritz method, written in the non-dimensionalised forms, become:

$$\begin{aligned}\Pi_S = \frac{1}{2}\int_0^1 \Bigg[&(-\psi^2 U + 2\psi W' + U'')^2 + \frac{6\beta^2}{1+\upsilon}(-\psi^2 U + 2\psi W' + U'')^2 \\ &+ \alpha(\psi^2 W + 2\psi U' - W'')^2 + \frac{6\beta^2}{1+\upsilon}(\psi^2 W + 2\psi U' - W'')^2\Bigg] d\xi\end{aligned} \tag{72}$$

$$\begin{aligned}\Pi_K = \frac{1}{2}\int_0^1 \lambda^2\Bigg[&-U^2 - W^2 + 2\mathrm{i}r^2(-1+\alpha)\eta\left(\psi W + U'\right)\left(\psi U - W'\right) \\ &+ r^2\eta^2\left(1+\alpha+\psi^2 U^2 + \alpha\left(\psi W + U'\right)^2 - 2\psi U W' + W'^2\right) \\ &- r^2(\alpha\psi^2 U^2 + (\psi W + U'^2) - 2\alpha\psi U W' + \alpha W'^2)\Bigg] d\xi\end{aligned} \tag{73}$$

Following the procedural step of the Rayleigh–Ritz method, we employ two approximating functions F_1 and F_2 to represent the original field variables U and W, respectively. Further, it is required that these approximating functions be a set of linearly independent function ϕ_i and ϑ_j for the field variables such that:

$$F_1 = \sum_{i=1}^{p} c_i \phi_i(\xi) \tag{74}$$

$$F_2 = \sum_{j=p+1}^{q} c_j \vartheta_j(\xi) \tag{75}$$

where c_i, $(i = 1, 2, \ldots, r)$ denote the generalised coordinates and ϕ_i and ϑ_j are unknown functions that satisfy the boundary conditions and also approximate the mode shapes. For the cantilever support conditions, we employ a set of approximating functions listed in Table 3.

Plugging the listed expressions in Table 3 in Equations (74) and (75) and then substituting Equations (74) and (75) into Equations (72) and (73), a residual functional in the form of the Rayleigh quotient of the system is obtained as:

Table 3. A list of approximating functions for the cantilever boundary condition.

	Approximating functions
$\phi_1 = \vartheta_1$	$(1-\xi)^2$
$\phi_2 = \vartheta_2$	$(1-\xi)^2\xi$
$\phi_3 = \vartheta_3$	$(1-\xi)^2(-0.5+\xi)\xi$
$\phi_4 = \vartheta_4$	$(1-\xi)^2(-0.75+\xi)(-0.25+\xi)\xi$
$\phi_5 = \vartheta_5$	$(1-\xi)^2(-0.8+\xi)(-0.5+\xi)(-0.2+\xi)\xi$
$\phi_6 = \vartheta_6$	$(1-\xi)^2(-0.84+\xi)(-0.6+\xi)(-0.34+\xi)(-0.18+\xi)\xi$

$$R\left[\mathcal{L}\left(\Pi_S, \Pi_K\right)\right] = \lambda^2 = \frac{\left(\Pi_S\right)_{\max}}{\left(\Pi_K\right)_{\max}} \tag{76}$$

By extremising Equation (76) with respect to the coefficients c_i, one arrives at:

$$\frac{\partial(\lambda^2)}{\partial c_i} = 0; \quad i = 1,\ 2,\ \ldots\ (p+q) \tag{77}$$

Equation (77) results in twelve homogeneous algebraic equations, which are then built into a complex eigenvalue problem using the matrix notation in the form:

$$\left[K - \lambda^2 M\right]\left\{c_i\right\} = \{\mathbf{0}\} \tag{78}$$

The non-trivial solutions of Equation (78) are obtained by using Wolfram's Mathematica®. For verification purpose, the accuracy of the solutions returned by the trial functions in Table 3 are assessed by comparing with the result of the transfer matrix method (TMM) reported in the recent study of Lee and Lee (2016) for one of the reduced model (non-spinning flexible beam with no rotary inertia, and no small-scale parameter). The comparison, and the excellent agreement, of the values is captured in Tables 4 and 5, for α = 10 and α = 100, respectively. It is seen from these tables that the presence of the pre-twist angle lowers (raises) the natural frequencies associated with odd-numbered (even-numbered) modes

Table 4. Effect of pre-twist angle on the non-dimensional natural frequencies of flexible beam with no rotary inertia.

	Rigidity ratio (α = **10**)					
	Present	TMM	Present	TMM	Present	TMM
ψ	1st	1st	2nd	2nd	3rd	3rd
0	3.516	3.516	11.119	11.119	22.034	22.035
10°	3.517	3.517	11.071	11.071	22.137	22.137
20°	3.521	3.521	10.935	10.935	22.438	22.438
30°	3.526	3.526	10.725	10.725	22.920	22.920
40°	3.534	3.534	10.460	10.460	23.560	23.560
50°	3.544	3.544	10.159	10.159	24.334	24.334
60°	3.556	3.556	9.839	9.839	25.216	25.216
70°	3.571	3.571	9.513	9.513	26.185	26.185
80°	3.587	3.587	9.189	9.189	27.218	27.218
90°	3.605	3.605	8.875	8.875	28.292	28.292

Table 5. Effect of pre-twist angle on the non-dimensional natural frequencies of flexible beam with no rotary inertia.

	Rigidity ratio ($\alpha = 100$)					
	Present	TMM	Present	TMM	Present	TMM
ψ	1st	1st	2nd	2nd	3rd	3rd
0	3.516	3.516	22.034	22.035	35.160	35.160
10°	3.517	3.517	21.579	21.579	35.880	35.880
20°	3.521	3.521	20.454	20.454	37.774	37.774
30°	3.527	3.527	19.056	19.056	40.358	40.358
40°	3.536	3.536	17.630	17.630	43.211	43.211
50°	3.547	3.547	16.285	16.285	45.865	45.863
60°	3.560	3.560	15.061	15.061	47.664	47.659
70°	3.576	3.576	13.969	13.969	48.121	48.113
80°	3.594	3.594	13.003	13.003	47.504	47.493
90°	3.614	3.614	12.152	12.152	46.335	46.321

Table 6. Effect of rotary inertia on the frequency values of vibration modes.

r	Mode 1	Mode 2	Mode 3	Mode 4
$\alpha = 1; \psi = 0°$				
0.000	3.516	3.516	22.034	22.034
0.050	3.496	3.496	21.191	21.191
0.100	3.437	3.437	19.136	19.136
0.150	3.344	3.344	16.748	16.748
0.200	3.226	3.226	14.576	14.576
		$\alpha = 10; \psi = 10°$		
0.000	3.517	11.071	22.137	60.870
0.050	3.496	10.486	21.249	51.207
0.100	3.433	9.145	19.118	34.585
0.150	3.335	7.711	16.684	25.743
0.200	3.209	6.500	14.500	20.538
		$\alpha = 10; \psi = 40°$		
0.000	3.534	10.460	23.560	54.703
0.050	3.495	10.031	22.076	47.126
0.100	3.384	9.000	18.965	34.466
0.150	3.216	7.837	16.025	26.331
0.200	3.010	6.815	13.746	21.187

of vibration. Moreover, the pre-twist angle effect is more pronounced for higher vibration modes.

Table 6 illustrates the decrease in the value of the natural frequencies with the consideration of the rotary inertia. The pattern of reduction of the natural frequency across the first four vibration modes is displayed in Figure 14. Table 6 and Figure 14 agree with the technical knowledge that ignoring the rotary inertia effect leads to an overestimation of the natural frequency values, especially for the higher vibration modes. Still, one can also see that for a fixed value of the rigidity ratio, the frequencies of the odd-numbered vibration modes is lessened as the pre-twist angle increases (the opposite happens for even-numbered modes). For instance, when $r = 0.2, \alpha = 10$, the fundamental frequency undergoes a reduction of 6.2% as ψ is increased from 10° to 40°, while the frequency of the second vibration mode increased by 4%. However, these changes shoot up when comparison is made with the model for which the rotary inertia effect is neglected. To see this,

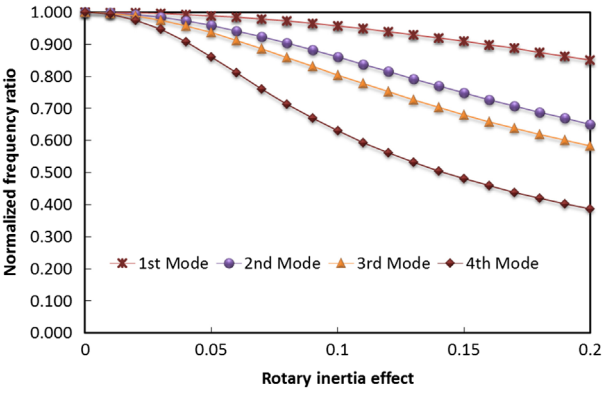

Figure 14. Visualisation of effect of rotary inertia on the vibration modes of the system.

Table 7. Effect of small-scale parameter on the frequency values of vibration modes.

		λ_1	λ_2	λ_3
$\beta = 0$	0.000	3.556	9.839	25.216
	0.050	3.498	9.529	23.071
	0.100	3.334	8.760	19.024
	0.150	3.100	7.842	15.700
	0.200	2.835	6.984	13.382
$\beta = 0.2$	0.000	3.882	10.135	26.991
	0.050	3.818	9.804	24.737
	0.100	3.638	8.989	20.393
	0.150	3.380	8.034	16.819
	0.200	3.087	7.155	14.324
$\beta = 0.5$	0.000	5.268	11.145	34.987
	0.050	5.180	10.741	32.049
	0.100	4.928	9.785	26.202
	0.150	4.558	8.723	21.360
	0.200	4.133	7.795	18.019

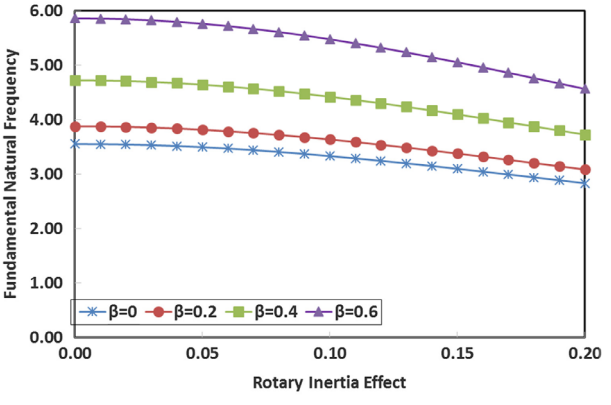

Figure 15. Visualisation of effect of small-scale parameter on the vibration modes of the system.

one may consider the case for which $r = 0.2, \alpha = 10$ and $\psi = 40^\circ$ (row 15). With these values, the frequency of the first vibration mode experiences a percentage reduction of14.82%, while the frequency of the second vibration mode decreased

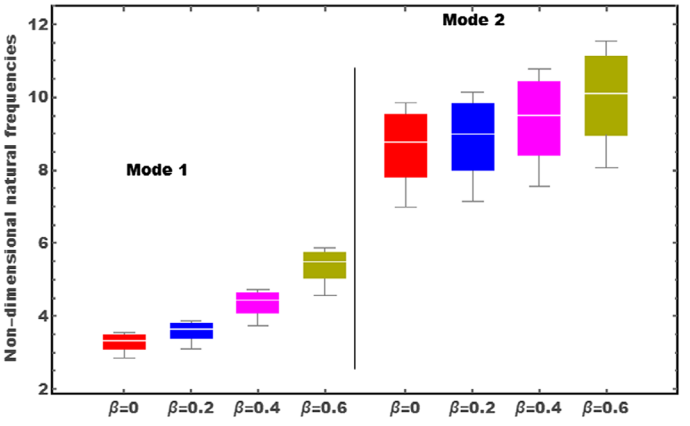

Figure 16. Assessment of the effect of small-scale parameter on the first and second vibration modes.

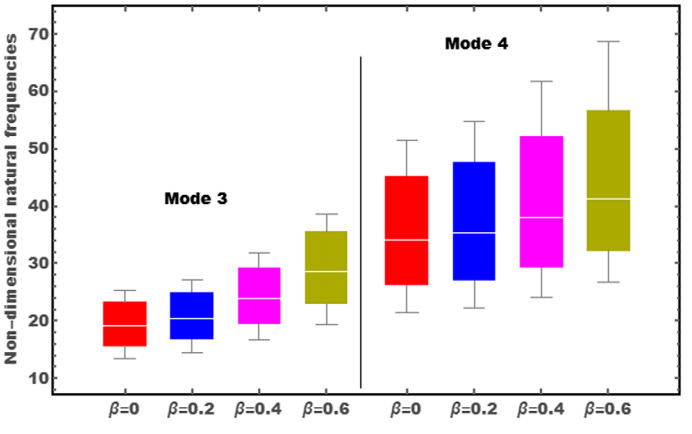

Figure 17. Assessment of the effect of small-scale parameter on the third and fourth vibration modes.

by 34.84%(in absolute value compared to when $r = 0$). Table 7 (supplemented by Figure 15) shows the trend of increment of the frequency values in the presence of the small-scale parameter. It is of interest to know that by increasing the small-scale parameter (β) from 0.2 to 0.5, the natural frequency experienced a percentage increase of roughly 33% (for $r = 0.2$ and other parameters kept as earlier mentioned). Figures 16 and 17 enhance the inference that the small-scale parameter, like the rotary inertia, imposes a greater influence on the higher modes of vibration.

5. Conclusion

The problem of analysing the spectral and vibration behaviours in a spinning pre-twisted micro-scale beam is considered. The spinning pre-twisted micro-scale beam is assumed to obey the Rayleigh beam theory, for which the rotary

inertia effect is important, and its scale-dependent property is accounted for with the MCST. The adopted variational formulation yields a set of partial differential equations that govern the coupled flexural dynamic behaviours of the system. For numerical analyses, the mathematical model is supplemented by higher order expressions for the shear force and bending moments of the micro-scale beam. The analyses carried out indicate the following:

- The presence of the pre-twist angle introduces bifurcation points that lead to the splitting of the elastic waves within the system. The frequency at which the bifurcation points occur increases with increasing values of the pre-twist angle and the small-scale parameter.
- There exist two pairs of non-zero cut-off frequencies for the coupled wave fields in the orthogonal planes system.
- The branches of the propagating wave increases from two to three as the pre-twist angle effect is taken into account, and this branching is related to the wave-splitting occurrence.
- The rotary inertia effect reduces the absolute value of the cut-off frequencies.
- The model based on the MCST indicates that the phase speed increases as the material length-scale parameter approaches the height of the cross section of the pre-twisted system.
- Finally, in comparison to the pre-twist and the small-scale parameter, the spinning parameter is found to have a very marginal effect on the dispersion and spectrum relations, but it has a very strong influence on the cut-off frequencies.
- Ignoring the rotary inertia effect leads to an overestimation of the natural frequency values for the higher vibration modes.
- The presence of the pre-twist angle lowers (raises) the natural frequencies associated with odd-numbered (even-numbered) modes of vibration.

Disclosure statement

No potential conflict of interest was reported by the author.

ORCID

K. B. Mustapha http://orcid.org/0000-0002-9905-9162

References

Abramowitz, M., & Stegun, I. A. (1965). *Handbook of mathematical functions*. New York, NY: Dover.

Aifantis, E. C. (1984). On the microstructural origin of certain inelastic models. *Journal of Engineering Materials and Technology, 106*, 326–330.

Aifantis, E. C. (1992). On the role of gradients in the localization of deformation and fracture. *International Journal of Engineering Science, 30*, 1279–1299.

Ataei, H., Beni, Y. T., & Shojaeian, M. (2016). The effect of small scale and intermolecular forces on the pull-in instability and free vibration of functionally graded nano-switches. *Journal of Mechanical Science and Technology, 30*, 1799–1816.

Balhaddad, A. S., & Onipede, D., Jr (1998). Three-dimensional free vibration of pretwisted beams. *AIAA Journal, 36*, 1524–1528.

Banerjee, J. R. (2001). Free vibration analysis of a twisted beam using the dynamic stiffness method. *International Journal of Solids and Structures, 38*, 6703–6722.

Banerjee, J. (2001). Free vibration analysis of a twisted beam using the dynamic stiffness method. *International Journal of Solids and Structures, 38*, 6703–6722.

Banerjee, J. R. (2001). Free vibration analysis of a twisted beam using the dynamic stiffness method. *International Journal of Solids and Structures, 38*, 6703–6722.

Banerjee, J. R. (2004). Development of an exact dynamic stiffness matrix for free vibration analysis of a twisted Timoshenko beam. *Journal of Sound and Vibration, 270*, 379–401.

Carnegie, W. (1957). Static bending of pre-twisted cantilever blading. *Proceedings of the Institution of Mechanical Engineers, 171*, 873–894.

Carnegie, W. (1959). Vibrations of pre-twisted cantilever blading. *Proceedings of the Institution of Mechanical Engineers, 173*, 343–374.

Carnegie, W. (1964). Vibrations of pre-twisted cantilever blading allowing for rotary inertia and shear deflection. *Journal of Mechanical Engineering Science, 6*, 105–109.

Challamel, N. (2013). Variational formulation of gradient or/and nonlocal higher-order shear elasticity beams. *Composite Structures, 105*, 351–368.

Chen, W.-R., & Chen, C.-S. (2015). Parametric instability of twisted Timoshenko beams with localized damage. *International Journal of Mechanical Sciences, 100*, 298–311.

Chen, W.-R., & Keer, L. (1993). Transverse vibrations of a rotating twisted timoshenko beam under axial loading. *Journal of Vibration and Acoustics, 115*, 285–294.

Chin, W. C. (2014). Overview and fundamental ideas. In *Wave propagation in drilling, well logging and reservoir applications* (pp. 1–49). Hoboken, NJ: Wiley.

Cosserat, E., & Cosserat, C. F. (1909). *Théorie des Corps Déformables*. Paris: A. Hermann et Fils.

Dawson, B. (1968). Coupled bending-bending vibrations of pre-twisted cantilever blading treated by the rayleigh ritz energy method. *Journal of Mechanical Engineering Science, 10*, 381–388.

Dehrouyeh-Semnani, A. M., Dehrouyeh, M., Torabi-Kafshgari, M., & Nikkhah-Bahrami, M. (2015). An investigation into size-dependent vibration damping characteristics of functionally graded viscoelastically damped sandwich microbeams. *International Journal of Engineering Science, 96*, 68–85.

Dehrouyeh-Semnani, A. M., Mostafaei, H., & Nikkhah-Bahrami, M. (2016). Free flexural vibration of geometrically imperfect functionally graded microbeams. *International Journal of Engineering Science, 105*, 56–79.

Deng, Y., Peng, L., Lai, X., Fu, M., & Lin, Z. (2017). Constitutive modeling of size effect on deformation behaviors of amorphous polymers in micro-scaled deformation. *International Journal of Plasticity, 89*, 197–222.

Doyle, J. F. (1997). *Wave propagation in structures : Spectral analysis using fast discrete Fourier transforms* (2nd ed.). New York, NY: Springer.

Eringen, A. C., & Edelen, D. G. B. (1972). On nonlocal elasticity. *International Journal of Engineering Science, 10*, 233–248.

Filiz, S., & Ozdoganlar, O. B. (2011). A three-dimensional model for the dynamics of micro-endmills including bending, torsional and axial vibrations. *Precision Engineering, 35*, 24–37.

Fleck, N. A., & Hutchinson, J. W. (1993). A phenomenological theory for strain gradient effects in plasticity. *Journal of the Mechanics and Physics of Solids, 41*, 1825–1857.

Fleck, N. A., Muller, G. M., Ashby, M. F., & Hutchinson, J. W. (1994). Strain gradient plasticity: Theory and experiment. *Acta Metallurgica et Materialia, 42*, 475–487.

Fu, C. (1974). Computer analysis of a rotating axial-turbomachine blade in coupled bending-bending-torsion vibrations. *International Journal for Numerical Methods in Engineering, 8*, 569–588.

Ghayesh, M. H., Farokhi, H., & Gholipour, A. (2017). Oscillations of functionally graded microbeams. *International Journal of Engineering Science, 110*, 35–53.

Ghorbani Shenas, A., Malekzadeh, P., & Ziaee, S. (2017). Thermal buckling of rotating pre-twisted functionally graded microbeams with temperature-dependent material properties. *Acta Mechanica, 228*, 1115–1133.

Ghorbani Shenas, A., Ziaee, S., & Malekzadeh, P. (2016). Vibrational behavior of rotating pre-twisted functionally graded microbeams in thermal environment. *Composite Structures, 157*, 222–235.

Gong, Y., Ehmann, K. F., & Lin, C. (2003). Analysis of dynamic characteristics of micro-drills. *Journal of Materials Processing Technology, 141*, 16–28.

Goodier, J. N., & Griffin, D. (1969). Elastic bending of pretwisted bars. *International Journal of Solids and Structures, 5*, 1231–1245.

Guglielmino, E., & Saccomandi, G. (1996). On the bending of pretwisted bars by a terminal transverse load. *International Journal of Engineering Science, 34*, 1285–1299.

Houbolt, J. C., & Brooks, G. W. (1957). *Differential equations of motion for combined flapwise bending* (TN 3905). NASA. Retrieved from Name website: https://ntrs.nasa.gov/search.jsp?R=19930092334

Hu, X. X., & Tsuiji, T. (1999). Free vibration analysis of curved and twisted cylindrical thin panels. *Journal of Sound and Vibration, 219*, 63–88.

Huang, B.-W., & Kuang, J.-H. (2007). The parametric resonance instability in a drilling process. *Journal of Applied Mechanics, 74*, 958–964.

Ilanko, S., Monterrubio, L., Mochida, Y. (2015). *The Rayleigh-Ritz method for structural analysis*. Hoboken, NJ: Wiley.

Karp, B., & Durban, D. (2005). Evanescent and propagating waves in prestretched hyperelastic plates. *International Journal of Solids and Structures, 42*, 1613–1647.

Lee, J., & Lee, J. (2016). Development of a transfer matrix method to obtain exact solutions for the dynamic characteristics of a twisted uniform beam. *International Journal of Mechanical Sciences, 105*, 215–226.

Leissa, A., MacBain, J., & Kielb, R. (1984). Vibrations of twisted cantilevered plates – Summary of previous and current studies. *Journal of Sound and Vibration, 96*, 159–173.

Leung, A. Y. T., & Fan, J. (2010). Natural vibration of pre-twisted shear deformable beam systems subject to multiple kinds of initial stresses. *Journal of Sound and Vibration, 329*, 1901–1923.

Leung, A., & Fan, J. (2010). Natural vibration of pre-twisted shear deformable beam systems subject to multiple kinds of initial stresses. *Journal of Sound and Vibration, 329*, 1901–1923.

Liang, L.-N., Ke, L.-L., Wang, Y.-S., Yang, J., & Kitipornchai, S. (2015). Flexural Vibration of an Atomic Force Microscope Cantilever Based on Modified Couple Stress Theory. *International Journal of Structural Stability and Dynamics, 15*, 1540025.

Liao, C. L., & Dang, Y. H. (1992). Structural characteristics of spinning pretwisted orthotropic beams. *Computers and Structures, 45*, 715–731.

Liew, K., Lim, C., & Ong, L. (1994). Vibration of pretwisted cantilever shallow conical shells. *International Journal of Solids and Structures, 31*, 2463–2476.

Lim, M. C., & Liew, K. (1995). Vibration of pretwisted cantilever trapezoidal symmetric laminates. *Acta Mechanica, 111*, 193–208.

Lin, S.-M., Wang, W.-R., & Lee, S.-Y. (2001). The dynamic analysis of nonuniformly pretwisted Timoshenko beams with elastic boundary conditions. *International Journal of Mechanical Sciences, 43*, 2385–2405.

Liu, K.-C., Friend, J., & Yeo, L. (2009). The axial–torsional vibration of pretwisted beams. *Journal of Sound and Vibration, 321*, 115–136.

Love, A. E. H. (1927). *A treatise on the mathematical theory of elasticity*. Cambridge: Cambridge Academic Press.

MacBain, J. C., Kielb, R. E., & Leissa, A. W. (1985). Vibrations of twisted cantilevered plates – Experimental investigation. *Journal of Engineering for Gas Turbines and Power, 107*, 187–196.

Mindlin, R. D., & Tiersten, H. F. (1962). Effects of couple-stresses in linear elasticity. *Archive for Rational Mechanics and Analysis, 11*, 415–448.

Mohammadimehr, M., Farahi, M. J., & Alimirzaei, S. (2016). Vibration and wave propagation analysis of twisted micro-beam using strain gradient theory. *Applied Mathematics and Mechanics, 37*, 1375–1392.

Mustapha, K. (2015). Coupled extensional-flexural vibration behaviour of a system of elastically connected functionally graded micro-scale panels. *European Journal of Computational Mechanics, 24*, 34–63.

Mustapha, K., & Hawwa, M. A. (2015). Eigenanalyses of functionally graded micro-scale beams entrapped in an axially-directed magnetic field with elastic restraints. *International Journal of Structural Stability and Dynamics, 16*, 1550022.

Mustapha, K. B., & Wong, B. T. (2016). Torsional frequency analyses of microtubules with end attachments. *ZAMM – Journal of Applied Mathematics and Mechanics/Zeitschrift für Angewandte Mathematik und Mechanik, 96*, 824–842.

Mustapha, K., & Zhong, Z. (2012). A new modeling approach for the dynamics of a micro end mill in high-speed micro-cutting. *Journal of Vibration and Control, 19*, 901–923. doi:10.1177/1077546312439912

Mustapha, K., & Zhong, Z. (2012). Wave propagation characteristics of a twisted micro scale beam. *International Journal of Engineering Science, 53*, 46–57.

Mustapha, K., & Zhong, Z. (2013). A hybrid analytical model for the transverse vibration response of a micro-end mill. *Mechanical Systems and Signal Processing, 34*, 321–339.

Pai, P. F., Qian, X., & Du, X. (2013). Modeling and dynamic characteristics of spinning Rayleigh beams. *International Journal of Mechanical Sciences, 68*, 291–303.

Prasolov, V. V. (2009). *Polynomials* (vol. 11). Berlin: Springer Science & Business Media.

Qatu, M. S., & Leissa, A. W. (1991). Vibration studies for laminated composite twisted cantilever plates. *International Journal of Mechanical Sciences, 33*, 927–940.

Rao, D. K. (1976). Transverse vibrations of pre-twisted sandwich beams. *Journal of Sound and Vibration, 44*, 159–168.

Razavilar, R., Alashti, R., & Fathi, A. (2014). Investigation of thermoelastic damping in rectangular microplate resonator using modified couple stress theory. *International Journal of Mechanics and Materials in Design, 12*, 1–13.

Reddy, J. N. (2002). *Energy principles and variational methods in applied mechanics* (2nd ed.). Hoboken, NJ: Wiley.

Reddy, J. N. (2011). Microstructure-dependent couple stress theories of functionally graded beams. *Journal of the Mechanics and Physics of Solids, 59*, 2382–2399.

Reissner, E., & Wan, F. Y. M. (1971). On stretching, twisting, pure bending and flexure of pretwisted elastic plates. *International Journal of Solids and Structures, 7*, 625–637.

Rosen, A. (1991). Structural and dynamic behavior of pretwisted rods and beams. *Applied Mechanics Reviews, 44*, 483–515.

Sahu, S., Asha, A., & Mishra, R. (2005). Stability of laminated composite pretwisted cantilever panels. *Journal of Reinforced Plastics and Composites, 24*, 1327–1334.

Shojaeian, M., Beni, Y. T., & Ataei, H. (2016). Electromechanical buckling of functionally graded electrostatic nanobridges using strain gradient theory. *Acta Astronautica, 118*, 62–71.

Şimşek, M., & Reddy, J. N. (2013). A unified higher order beam theory for buckling of a functionally graded microbeam embedded in elastic medium using modified couple stress theory. *Composite Structures, 101*, 47–58.
Sinha, S. K., & Turner, K. E. (2011). Natural frequencies of a pre-twisted blade in a centrifugal force field. *Journal of Sound and Vibration, 330*, 2655–2681.
Song, O., Jeong, N.-H., & Librescu, L. (2000). Vibration and stability of pretwisted spinning thin-walled composite beams featuring bending–bending elastic coupling. *Journal of Sound and Vibration, 237*, 513–533.
Subrahmanyam, K., Kulkarni, S., & Rao, J. (1981). Coupled bending-bending vibrations of pre-twisted cantilever blading allowing for shear deflection and rotary inertia by the Reissner method. *International Journal of Mechanical Sciences, 23*, 517–530.
Tekinalp, O., & Ulsoy, A. (1989). Modeling and finite element analysis of drill bit vibrations. *Journal of Vibration Acoustics Stress and Reliability in Design, 111*, 148–155.
Toupin, R. A. (1964). Theories of elasticity with couple-stress. *Archive for Rational Mechanics and Analysis, 17*, 85–112.
Troesch, A., Anliker, M., & Ziegler, H. (1954). Lateral vibrations of twisted rods. *Quarterly of Applied Mathematics, 12*, 163–173.
Wajchman, D., Liu, K. C., Friend, J., & Yeo, L. (2008). An ultrasonic piezoelectric motor utilizing axial-torsional coupling in a pretwisted non-circular cross-sectioned prismatic beam. *IEEE Transactions on Ultrasonics, Ferroelectrics, and Frequency Control, 55*, 832–840.
Watson, B., Friend, J., & Yeo, L. (2009). Micromotor of less than 1 mm^3 volume for in vivo medical procedures. In *Quantum, Nano and Micro Technologies, 2009 ICQNM '09. Third International Conference on*, 2009 (pp. 81–85).
Yang, J. F. C., & Lakes, R. S. (1982). Experimental study of micropolar and couple stress elasticity in compact bone in bending. *Journal of Biomechanics, 15*, 91–98.
Yang, F., Chong, A. C. M., Lam, D. C. C., & Tong, P. (2002). Couple stress based strain gradient theory for elasticity. *International Journal of Solids and Structures, 39*, 2731–2743.
Yardimoglu, B., & Inman, D. J. (2004). Coupled bending-bending-torsion vibration of a rotating pre-twisted beam with aerofoil cross-section and flexible root by finite element method. *Shock and Vibration, 11*, 637–646.
Young, T., & Gau, C. (2003). Dynamic stability of spinning pretwisted beams subjected to axial random forces. *Journal of Sound and Vibration, 268*, 149–165.
Zeighampour, H., & Beni, Y. T. (2015). A shear deformable cylindrical shell model based on couple stress theory. *Archive of Applied Mechanics, 85*, 539–553.
Zeighampour, H., Beni, Y. T., & Mehralian, F. (2015). A shear deformable conical shell formulation in the framework of couple stress theory. *Acta Mechanica, 226*, 2607–2629.
Zhang, W.-M., & Meng, G. (2006). Stability, bifurcation and chaos of a high-speed rub-impact rotor system in MEMS. *Sensors and Actuators A: Physical, 127*, 163–178.
Zickel, J. (1952). Bending of pretwisted beams. *DTIC Document*.

Appendix 1

$$C_1 = \frac{(1+6\beta^2+\upsilon)(\alpha+6\beta^2+\alpha\upsilon)}{(1+\upsilon)^2}$$

$$C_2 = -\frac{r^2\lambda^2(1+\upsilon)(6\beta^2(1+\eta^2)+\eta^2(1+\upsilon)+\alpha^2\eta^2(1+\upsilon)+2\alpha(1+3\beta^2(1+\eta^2)+\upsilon))+4(1+6\beta^2+\upsilon)(\alpha+6\beta^2+\alpha\upsilon)\psi^2}{(1+\upsilon)^2}$$

$$C_3 = -\frac{2r^2(1+\alpha)\eta\lambda^2(1+\alpha+12\beta^2+\upsilon+\alpha\upsilon)\psi}{1+\upsilon}$$

$$C_4 = \frac{1}{(1+\upsilon)^2}(r^4\alpha(-1+\eta^2)^2\lambda^4(1+\upsilon)^2 + 6(1+6\beta^2+\upsilon)(\alpha+6\beta^2+\alpha\upsilon)\psi^4 + \lambda^2(1+\upsilon)(r^2\alpha^2(-1+2\eta^2)(1+\upsilon)\psi^2 + 6\beta^2(-2+r^2(1+\eta^2)\psi^2) + (1+\upsilon)(-1+r^2(-1+2\eta^2)\psi^2) - \alpha(1-2r^2(2-\eta^2+3\beta^2(1+\eta^2))\psi^2 + \upsilon(1+2r^2(-2+\eta^2)\psi^2))))$$

$$C_5 = \frac{4r^2(1+\alpha)\eta\lambda^2(1+\alpha+12\beta^2+\upsilon+\alpha\upsilon)\psi^3}{1+\upsilon}$$

$$C_6 = \frac{1}{(1+\upsilon)^2}(-2r^4\alpha(-1+\eta^2)^2\lambda^4(1+\upsilon)^2\psi^2 - 2\psi^2(3\lambda^2(1+\upsilon)(1+\alpha+12\beta^2+\upsilon+\alpha\upsilon) + 2(1+6\beta^2+\upsilon)(\alpha+6\beta^2+\alpha\upsilon)\psi^4) + r^2\lambda^2(1+\upsilon)((1+\alpha)(1+\eta^2)\lambda^2(1+\upsilon) + (6\beta^2(1+\eta^2) - (-2+\eta^2)(1+\upsilon) - \alpha^2(-2+\eta^2)(1+\upsilon) + \alpha(6\beta^2(1+\eta^2) + 2(-1+2\eta^2)(1+\upsilon)))\psi^4))$$

$$C_7 = -\frac{2r^2(1+\alpha)\eta\lambda^2\psi(2\lambda^2(1+\upsilon) + (1+\alpha+12\beta^2+\upsilon+\alpha\upsilon)\psi^4)}{1+\upsilon}$$

$$C_8 = \frac{1}{(1+\upsilon)^2}((1+6\beta^2+\upsilon)(\alpha+6\beta^2+\alpha\upsilon)\psi^8 + \lambda^4(1+\upsilon)^2(1+r^2(1+\alpha)(1+\eta^2)\psi^2 + r^4\alpha(-1+\eta^2)^2\psi^4) - \lambda^2(1+\upsilon)\psi^4(r^2\alpha^2(1+\upsilon)\psi^2 + (1+\upsilon)(1+r^2\psi^2) + 6\beta^2(2+r^2(1+\eta^2)\psi^2) + \alpha(1+\upsilon+2r^2(\eta^2+3\beta^2(1+\eta^2))\psi^2 + 2r^2\eta^2\upsilon\psi^2)))$$

$$Q_1 = 1 + k^4r^4\alpha(-1+\eta^2)^2 - 4kr^2(1+\alpha)\eta\psi + r^2(1+\alpha)(1+\eta^2)\psi^2 + r^4\alpha(-1+\eta^2)^2\psi^4 + k^2r^2(1+\eta^2+\alpha(1+\eta^2-2r^2\psi^2+4r^2\eta^2\psi^2-2r^2\eta^4\psi^2$$

$$Q_2 = -\frac{1}{1+\upsilon}(k^6r^2(6\beta^2(1+\eta^2)+\eta^2(1+\upsilon)+\alpha^2\eta^2(1+\upsilon)+2\alpha(1+3\beta^2(1+\eta^2)+\upsilon)) + 2k^5r^2(1+\alpha)\eta(1+\alpha+12\beta^2+\upsilon+\alpha\upsilon)\psi - 4k^3r^2(1+\alpha)\eta(1+\alpha+12\beta^2 + \upsilon+\alpha\upsilon)\psi^3 + 2kr^2(1+\alpha)\eta(1+\alpha+12\beta^2+\upsilon+\alpha\upsilon)\psi^5 + \psi^4(r^2\alpha^2(1 + \upsilon)\psi^2 + (1+\upsilon)(1+r^2\psi^2) + 6\beta^2(2+r^2(1+\eta^2)\psi^2) + \alpha(1+\upsilon+2r^2(\eta^2 + 3\beta^2(1+\eta^2))\psi^2 + 2r^2\eta^2\upsilon\psi^2)) + k^2\psi^2(r^2\alpha^2(-2+\eta^2)(1+\upsilon)\psi^2 + (1 + \upsilon)(6+r^2(-2+\eta^2)\psi^2) - 6\beta^2(-12+r^2(1+\eta^2)\psi^2) + \alpha(6-2r^2(-1 + 2\eta^2+3\beta^2(1+\eta^2))\psi^2 + \upsilon(6+2r^2(1-2\eta^2)\psi^2))) - k^4(r^2\alpha^2(-1 + 2\eta^2)(1+\upsilon)\psi^2 + 6\beta^2(-2+r^2(1+\eta^2)\psi^2) + (1+\upsilon)(-1+r^2(-1 + 2\eta^2)\psi^2) - \alpha(1-2r^2(2-\eta^2+3\beta^2(1+\eta^2))\psi^2 + \upsilon(1+2r^2(-2+\eta^2)\psi^2)))$$

$$Q_3 = \frac{(1+6\beta^2+\upsilon)(\alpha+6\beta^2+\alpha\upsilon)(k^2-\psi^2)^4}{(1+\upsilon)^2}$$